

Original Article

Acteoside exerts neuroprotective effects by preventing α -synuclein aggregation and oxidative stress in models of Parkinson's disease

Alessia Lambiase^{a,b}, Giorgia Spandri^a, Hind Moukham^a, Elisa Toini^{a,b}, Annalisa D'Urzo^a, Giovanni Zecca^{a,b}, Mauro Commisso^{b,c}, Flavia Guzzo^{b,c}, Valentina Santoro^{d,b}, Anna Lisa Piccinelli^{d,b}, Enrica Calleri^{e,b}, Sofia Salerno^e, Francesca Rinaldi^e, Stefano Negri^{b,c}, Carlo Santambrogio^a, Maura Brioschi^a, Cristina Solana-Manrique^{f,g}, Massimo Labra^{a,b}, Fabrizio Grassi^{a,b}, Nuria Paricio^f, Farida Tripodi^{a,b}, Paola Coccetti^{a,b,*}

^a Department of Biotechnology and Biosciences, University of Milano-Bicocca, Milano, Italy

^b National Biodiversity Future Center (NBFC), Palermo, Italy

^c Department of Biotechnology, University of Verona, Verona, Italy

^d Department of Pharmacy, University of Salerno, Fisciano, Italy

^e Department of Drug Sciences, University of Pavia, Italy

^f Department of Genetics and University Institute of Biotechnology and Biomedicine, University of Valencia, Spain

^g Department of Physiotherapy, European University of Valencia, Spain

ARTICLE INFO

Keywords:

Verbascum thapsus

Verbascoside

Lifaspan

Saccharomyces cerevisiae

Drosophila melanogaster

ABSTRACT

α -Synuclein is a small presynaptic protein whose aggregation is one of the hallmarks of Parkinson's disease (PD). In our quest to identify novel preventive or therapeutic treatments for PD, we collected 60 Italian plant species, representative of part of the Mediterranean flora, which were screened by a phylogenetic analysis in conjunction with a high-throughput screening in a yeast model of PD expressing human α -synuclein. The integration of these approaches led to the identification of four plants, *Allium lusitanicum*, *Salvia pratensis*, *Verbascum thapsus* and *Glaucium flavum*, whose extracts, characterized by a metabolomic analysis, exhibit robust inhibitory activity against the amyloid aggregation of α -synuclein *in vitro*, as well as in neuroblastoma cells overexpressing the protein. By employing a size exclusion chromatography affinity approach coupled to mass spectrometry, we identified the phenylpropanoid glycoside acteoside from the extract of the edible plant *V. thapsus* as the metabolite that directly binds α -synuclein and effectively inhibits its fibril formation. In addition, acteoside reduces oxidative stress in neuroblastoma cells exposed to α -synuclein fibrils and activates the NRF2 pathway. Notably, acteoside improves motor performance in a *Drosophila* model of PD and exhibits a significant reduction of protein carbonyl groups, suggesting that this compound may mitigate oxidative stress-induced protein damage. Our findings could pave the way for the development of new strategies aimed at discovering novel neuroprotective agents targeting PD-related diseases.

Introduction

Aging is a complex physiological condition influenced by various biological pathways that not only affect lifespan but also play a crucial role in the development and progression of age-related diseases. Among these, Parkinson's disease (PD) is a neurodegenerative disorder affecting 2–3 % of the population over 65 years, clinically characterized by movement disorders and cognitive impairment, and by the misfolding and aggregation of α -synuclein at the molecular level [1–3]. α -Synuclein (α -syn) is a small presynaptic protein, mainly expressed in neurons of the

central and peripheral nervous system, involved in the regulation of vesicle trafficking and neurotransmitter release [4]. It is an intrinsically disordered protein that can adopt an α -helical conformation when associated with biological membranes. Mutations or overexpression of α -syn can lead to aggregation into toxic oligomers and fibrils, which alter vesicle trafficking, mitochondrial activity and induce cellular toxicity, ultimately leading to the loss of dopaminergic neurons [2].

The onset of age-related diseases is also shaped by environmental factors. According to the One Health concept, the health of humans, animals, plants, and the environment are closely linked and inter-dependent, and by

* Corresponding author.

E-mail address: paola.coccetti@unimib.it (P. Coccetti).

<https://doi.org/10.1016/j.neurot.2025.e00825>

Received 4 September 2025; Received in revised form 19 November 2025; Accepted 8 December 2025

1878-7479/© 2025 The Author(s). Published by Elsevier Inc. on behalf of American Society for Experimental NeuroTherapeutics. This is an open access article under the CC BY-NC-ND license (<http://creativecommons.org/licenses/by-nc-nd/4.0/>).

means of a collaborative and *trans*-disciplinary approach it aims to achieve improved health and well-being outcomes. Through the bioprospecting approach, biodiversity enables the identification of a number of compounds (from diverse sources such as plants, marine organisms, and microorganisms) with bioactive properties beneficial for preventing or treating human diseases. Indeed, the potential of natural compounds is huge, and recent years have seen a surge in publications highlighting their numerous neuroprotective effects [5,6]. In this context, selecting plant candidates is a critical step before analyzing their biological activities. As Najmi et al. [7] suggested, various approaches can be employed: selection based on ethnopharmacological knowledge, traditional medicine systems, or random selection. However, it has been suggested that closely related taxa may share biosynthetic pathways of similar phyto-metabolites and that their chemical molecules are generally conserved with each other [8, 9]. Molecular phylogenetic approaches offer an alternative method to identify plant-based natural products reducing the time and cost of subsequent biological analysis [9,10].

The National Biodiversity Future Center in Italy is dedicated to conserving, restoring, monitoring, and enhancing biodiversity within the Mediterranean biodiversity hotspot [11] (<https://www.nbfc.it>). The Mediterranean basin, with its diverse and heterogeneous plant life, boasts a significant number of endemic species, likely due to its varied geography, environmental conditions, and historical influences [12]. Although many Mediterranean plants have been described, they remain a vital resource for research in biochemistry, phytochemistry, and pharmacology, potentially leading to the discovery of new therapeutic molecules.

This study was designed to develop an innovative integrated approach to select the most promising neuroprotective plant extracts from a library of Mediterranean plants. We exploited the information present in a broad phylogenetic framework, combined with a high-throughput screening in a yeast model of PD expressing human α -syn. From the selected plant extracts, we identified the phenylpropanoid glycoside acteoside, with strong anti-aggregant activity against α -syn fibrillation. The neuroprotective properties of acteoside were deeply evaluated through biophysical techniques, in neuroblastoma cell cultures and in a *Drosophila melanogaster* model of PD based on the inactivation of the *DJ-1 β* gene [13], the fly ortholog of human *DJ-1* (*PARK7*), mutated in early-onset familial PD forms [14].

Materials and methods

Sample collection and extraction

Aerial vegetative organs (leaves and eventually young herbaceous stems) of the 60 plant species investigated were collected in triplicate from plants growing in the botanical garden of Padova (Italy), grown in a nursery or in the open field, as specified in [Supplementary Table S1](#). The samples were immediately frozen in liquid nitrogen, ground into a fine powder using an A11 basic analytical mill (IKA-Werke, Staufen, Germany), and then stored at -80°C . Approximately 1 g of frozen powder was subjected to extraction using 10 vol (w/v) of 100 % LC-MS grade methanol (Honeywell, Seelze, Germany). The mixture was vortexed for 30 s, sonicated on ice for 10 min in a 40-kHz ultrasonic bath (SOLTEC, Milano, Italy), and then centrifuged at 14,000 g for 10 min at 4°C . The collected supernatants were divided into ten 1.5 mL tubes, with each tube containing 1 mL of extract, and stored at -20°C . Nine aliquots were then subjected to processing with a vacuum evaporation system (SpeedVac, Heto-Holten, Frederiksberg, Denmark) and allocated for the following *in vitro* bioassays, while one aliquot was kept for LC-MS analysis.

Untargeted liquid chromatography-mass spectrometry (LC-MS) metabolomics analysis

The untargeted LC-MS metabolomics analyses were performed using the instrumentation and methodology described in previous studies [15, 16] with slight modifications. In brief, the extracts were diluted at 1:10, 1:50 and 1:100 with LC-MS grade water (Honeywell) and filtered

through $0.22\ \mu\text{m}$ Minisart filters (Sartorius-Stedim Biotech, Göttingen, Germany). The analyses were performed with Ultra-Performance Liquid Chromatography-High-Resolution Mass Spectrometry (UPLC-HRMS) and 5 and $1\ \mu\text{L}$ were injected into the instrument for analysis in both negative and positive ionization modes, respectively. The elution was carried out in gradient mode among two mobile phases (A: 0.1 % formic acid in water, B: 100 % acetonitrile). The elution gradient commenced at 1 % B, held for 1 min, then increased to 40 % B at 10 min, 70 % B at 13.5 min, 90 % B at 15 min, and reached 99 % B at 16.5 min. The method was then maintained at 99 % B for 3.5 min before returning to 1 % B at 20.1 min. The method concluded with an isocratic phase (1 % B) at 25 min. MS data were acquired in profile and sensitivity modes and by using a scan range of 50–2000 *m/z*. The scan time was set at 0.3 s and the MS data were acquired with function 1 (no fragmentation) and function 2 (CID fragmentation with argon at 35 eV). Furthermore, a FAST-DDA data-dependent analysis was conducted to improve metabolite identification. This involved assessing the accurate mass (derived from the *m/z* ratio), retention time, and fragmentation pattern (MS/MS from the FAST-DDA analysis) for each ion, followed by cross-referencing with a proprietary library of authentic standard compounds, an *in silico* database of plant compounds, and relevant scientific literature and public databases such as Pubchem, MoNA and MassBank. Identification levels were established according to metabolomics standards initiative (MSI): level 1, unambiguous identification with reference standards; level 2, putative assignment based on MS data similarity with literature data or databases; level 3, putative assignment established by spectral similarity to chemical class of compounds and chemotaxonomic data.

Phylogenetic selection approach

The lists of plants with anti-aggregant, neuroprotective and anti-Parkinson's biological activities were downloaded from the Dr. Duke's Phytochemical and Ethnobotanical Databases [17,18] to determine their phylogenetic clumping. Hereinafter, we will refer to these plants as 'Medicinal Plants' (MP). The MP belonging to the Pteridophyta and Ceratophyllales ([Supplementary Table S1](#)) were excluded from the phylogenetic analyses due to their low number in the database. The Maximum Likelihood (ML)-based chronogram produced by Zanne et al. [19] was downloaded and four monophyletic subtrees (i.e., Monocotyledoneae with 7060 tips, Superrosidae with 10,009 tips, Superasteridae with 11,324 tips, and Basal eudicots with 948 tips as defined in Ref. [19]) representing 29,341 species in total, were extracted for use as reference in subsequent analyses.

The functions available in the R package 'pm4mp' (<https://github.com/gzecca/pm4mp>) were used as follows. The function "*clean_and_match()*" was applied with the argument "*reftype = z*" and the argument "*match_thr = 0.9*" to standardise the species names and to find the fuzzy matches between the MP names and tree tip names. The resulting fuzzy matches were manually checked for misspelling on the Plants of the World Online (<https://www.plantsoftheworldonline.org>) and on the World Flora Online (<https://www.worldfloraonline.org>) databases and corrected when necessary in the MP lists ([Supplementary Table S2](#)). The "*tree4nodesigl()*" and "*sample4nodesigl()*" functions were used to prepare input files for PHYLOCOM v4.2, which was used to identify the "*hot nodes*" in the reference phylogenies [20]. The "*hot nodes*" are the nodes on a phylogenetic tree that contain an overabundance of taxa of a given category compared to a random pattern of distribution [21,22]. The function "*nodesiglR()*" with parameters "*start = 1*" and "*stop = 1500*" was used to run PHYLOCOM from R and to perform 1500 repetitions of the "*nodesigl*" command using 999 randomizations each. Repetitions were necessary because of the stochastic nature of the null model used by PHYLOCOM to test the statistical significance of hot nodes. The appropriate number of repetitions was determined based on preliminary analyses, and chosen to exceed the number of replicates after which the detected *hot nodes* remained constant (data not shown). The function "*nodesigl_harvesteR()*" with the

argument “*fract* = 5” was used to keep the (stable) *hot nodes* present in all 1500 runs that contained at least 5 % of MPs and to extract their corresponding “*hot trees*” in Newick format. We define the “*hot trees*” as subtrees of the reference phylogenies containing independent subsets of phylogenetically nested “*hot nodes*” and therefore containing different sets of species (for details see the “*pm4mp*” package documentation). The 60 plant species selected by the NBFC project (Supplementary Tables S1 and S2) were searched within the identified *hot trees*. The “*hot-tree-painteR()*” function was used to plot the *hot trees* where at least one plant species selected by the NBFC project was found.

Yeast strains and media

The yeast strain utilized to assess the biological activity of plant extracts is BY4742[pYX242-SNCA], overexpressing human α -syn. Cell cultures were grown in minimal medium containing 2 % glucose as the carbon source and 0.67 % yeast nitrogen base lacking amino acids, supplemented with 50 mg/L of essential amino acids and bases necessary for the auxotrophic strain’s requirements and with 0.1 mM ampicillin to prevent contaminations. Cells were grown at 30 °C under continuous agitation at 120 rpm. For treatments with the extracts, the dried extracts, obtained by 100 mg of fresh leaves, were resuspended in 75 μ L of 100 % ethanol, vortexed and sonicated for 20 min at 28 KHz and then added to 5 mL of the medium. In the control condition, 75 μ L of ethanol was added in the medium (final ethanol concentration of 1.5 %).

Biolog OmniLog system

The Biolog OmniLog System was utilized to compare the cellular phenotypes of BY4742[pYX242-SNCA] yeast cells supplemented with 60 different extracts. Yeast cell cultures were grown on agar plates at 30 °C, then inoculated into 8 mL of 2 % glucose minimal medium in sterile glass tubes. The cell suspension was measured using the BIOLOG Turbidimeter (Biolog, Hayward, CA) until reaching a cell suspension transmittance of 62 % T. The suspension was prepared according to the BIOLOG PM protocol for yeast cells: Dye D 75x (Biolog, Hayward, CA), cells 48x, and medium. This suspension was then pipetted into the 96-well plates (100 μ L per well). All dried extracts were resuspended in 75 μ L of 100 % EtOH and 1.5 μ L of extract, corresponding to 20 mg of fresh leaves/mL medium, were added to each well of the plates (1.5 % EtOH final concentration) to reach a 100 μ L total volume. Microplates were then incubated in the OmniLogTM system at 30 °C for 72 h. The experiment was conducted in triplicate. Growth profiles were compared using the y-maximum value of each kinetic curve.

Chronological lifespan assay (CLS)

Cells were grown in liquid medium until reaching the mid-late exponential phase, after which they were inoculated at a density of 0.150 OD/mL into flasks containing medium either without extracts (solvent control) or supplemented with the extract (corresponding to 20 mg of fresh leaves/mL medium). Survival (expressed as percentage) was evaluated by propidium iodide (PI) staining at different time points using the Cytoflex cytofluorimeter (Beckman Coulter, Milan, Italy) and analyzed with Cytoflex software (version 2.6.0.105), as previously reported [23].

Analysis of reactive oxygen species (ROS) and aggresome levels in yeast

ROS level within the cells was assessed through DHE (dihydroethidium) staining. Following a 24 h treatment with the extracts, cells were harvested, resuspended in phosphate-buffered saline (PBS) solution, and stained with 5 μ g/mL of DHE for 10 min, as previously reported [23]. Flow cytometric analyses were conducted using the Cytoflex cytofluorimeter (Beckman Coulter) and data were analyzed using Cytoflex software (version 2.6.0.105). The intracellular protein aggresomes were analyzed using the PROTEOSTAT[®] Aggresome detection kit (ENZO Life

Sciences). Yeast cells were collected after 24 h treatment with the extracts; 0.2 OD of cells were collected and resuspended in PBS buffer and stained with the PROTEOSTAT[®] Aggresome detection reagent at a dilution of 1:1500, as previously reported [24]. Fluorescence-activated cell sorting (FACS) analyses were conducted using a Cytoflex cytofluorimeter (Beckman Coulter) and analyzed with Cytoflex software.

Thioflavin T (ThT) assay

α -syn was purchased from Merck-Millipore and dissolved at 70 μ M in PBS. Protein samples (20 μ L, 70 μ M concentration of α -syn) were incubated at 37 °C in PBS up to 72 h under constant shaking at 900 rpm with a thermo-mixer in the absence (cnt) or in the presence of the extracts. Dried extracts, corresponding to 100 mg of fresh leaves resuspended in 75 μ L of 100 % ethanol, were diluted 1:10 in PBS and 5 μ L were added to α -syn to test their effect on protein aggregation; in control experiments ethanol was used as solvent control. The ThT binding assay was performed according to Ref. [25] using a 20 μ M ThT solution in the PBS buffer. 180 μ L of ThT solution were added to 20 μ L of the aggregated α -syn samples, transferred into a black 96-well clear bottom multiwell plate and ThT fluorescence was read at the maximum intensity of fluorescence of 485 nm using a Victor X3 plate reader (PerkinElmer). Fluorescence of blank samples was subtracted from the fluorescence values of all samples. In control experiments with each extract, no interference with ThT fluorescence was observed.

Seed fibrils formation

For seed fibrils formation 250 μ L of α -syn at 70 μ M was incubated at 37 °C in PBS for 72 h under constant shaking at 900 rpm in a thermo-mixer. Fibrils formation was verified through the Thioflavin T assay by mixing 10 μ L of fibril samples with 20 μ M ThT in a final volume of 100 μ L. Fluorescence emission at 485 nm was recorded using a plate reader (BioTek Synergy H1, Agilent).

Aggregation kinetics

For kinetic experiments, 35 μ M α -syn (100 μ L) was incubated at 37 °C in PBS, with 20 μ M ThT solution in PBS, up to 72 h under constant shaking at 425 cpm using a plate reader (BioTek Synergy H1, Agilent) in the absence (cnt) or in the presence of *V. thapsus* extract or acteoside (50 μ M and 100 μ M). The dried extract of *V. thapsus* was resuspended in 75 μ L of 100 % EtOH and 2.5 μ L were added to α -syn to test the effect on protein aggregation; in control experiments ethanol was used as solvent control. For fibril elongation experiments, 1 μ M preformed seed fibrils were added to 35 μ M α -syn in PBS. To probe fibril elongation, protein samples (100 μ L) were incubated at 37 °C in PBS, with 20 μ M ThT solution in PBS, under constant shaking at 425 cpm using a plate reader (BioTek Synergy H1, Agilent) in the absence (cnt) or in the presence of acteoside (1 μ M, 25 μ M, 50 μ M and 100 μ M). Acteoside was purchased from Merck and was resuspended in water and added to α -syn; in control experiments water was used as solvent control.

Transmission electron microscopy (TEM) imaging

For the visualization of α -syn fibrils by TEM, α -syn was used at 70 μ M in PBS. Protein samples (250 μ L) were incubated at 37 °C in PBS, with 20 μ M ThT solution in PBS under constant shaking at 900 rpm with a thermo-mixer up to 72 h, in absence (cnt) or in the presence of acteoside (50 μ M). Samples were loaded on carbon coated copper TEM grids (5 μ L) and let them air-dried. Then a negative staining (Uranyl Acetate, 1 %) was performed to enhance the contrast and to improve the observations. TEM micrographs were acquired with JEOL JEM 2100Plus Transmission Electron Microscope (JEOL, Japan) operating with an acceleration voltage of 200 kV, and equipped with an 8 megapixel Gatan (Gatan, USA) Rio Complementary Metal-Oxide-superconductor (CMOS) camera.

Cell cultures

SH-SY5Y cell lines harboring *pTet-SNCA-FLAG* were purchased from Merck. Cells were cultured on plates at 37 °C in DMEM/F12 medium, containing 10 % fetal bovine serum, 2 mM glutamine, 100 units/mL penicillin and 100 µg/mL streptomycin, in a humidified 5 % CO₂ incubator. Doxycycline-inducible α-syn-expressing cells were selected against the antibiotic puromycin with a dose of 2 µg/mL. Induction of α-syn expression was achieved by adding 6 µg/mL doxycycline (from a 6 mg/mL stock in DMSO) for 48 h.

The extracts obtained from 100 mg of fresh leaves were resuspended in 75 µL of 100 % ethanol and used as 200x stocks (corresponding to 6.6 mg/mL of medium, final ethanol concentration 0.5 %); 0.5 % ethanol was used as solvent control. Acteoside was resuspended in water and used at a final concentration of 100 µM. For immunofluorescence assays, 1.6×10^5 cells were seeded on geltrex-coated glass cover slips in wells of a 24 multiwell plate and treated the day after for 48 h.

SH-SY5Y cells were purchased from ATCC. Cells were cultured on plates at 37 °C in DMEM medium, containing 10 % fetal bovine serum, 2 mM glutamine, 100 units/mL penicillin and 100 µg/mL streptomycin, in a humidified 5 % CO₂ incubator. For analysis of ROS level 8×10^3 cells were seeded in wells of a 96 multiwell plate and treated with 5 µM of α-syn fibrils for 72 h. To obtain the fibrils, α-syn (70 µM) was incubated at 37 °C in PBS up to 72 h under constant shaking at 900 rpm with a thermo-mixer in the presence or in the absence of acteoside (1 mM).

Analysis of acteoside availability in cells

To evaluate the intracellular/cell-associated level of acteoside, 2×10^6 SH-SY5Y *pTet-SNCA-FLAG* cells were seeded in 60-mm dishes and treated with acteoside at 100 µM up to 24 h. For metabolite extraction, cells were washed twice with PBS before being lysed with ice cold 80 % methanol solution for 5 min. The lysate was transferred into a 1.5 mL tube and sonicated in bath 1 min on and 1 min off for 5 times. Samples were centrifuged at 14,000 g for 30 min at 4 °C and the supernatant was filtered using a 3 kDa molecular weight cut-off filter at 14000 g for 1 h at 4 °C. The eluate was transferred in LC-MS vials and stored at -20 °C.

Samples were injected into a Xevo G2-XS quadrupole time of flight mass spectrometer coupled to a Waters ACQUITY ultra-performance liquid chromatography (UPLC) H-Class system through an ESI source (Waters Corporation, Milford, MA, USA). The instrument was operated in negative ion current in sensitivity mode. The capillary voltage was maintained at 1.5 kV with the source temperature held constant at 140 °C.

An ACQUITY UPLC® BEH C18 1.7 µm, 2.1 mm × 50 mm, (Waters Corporation, Milford, MA, USA) was used for analyte separation. The flow rate was set to 400 µL/min with a column temperature of 40 °C. A gradient of solvent A (99.9 % LC-MS-grade water with 0.1 % formic acid) and solvent B (LC-MS-grade 99.9 % acetonitrile with 0.1 % formic acid) was applied with a total run time of 12 min as follows: 0–0.3 min at 2 % B; 0.3–6.3 min linear increase from 2 to 98 % B; 6.3–8.3 min 98 % B; 9–12 min 2 % B. Transition selection and optimization of collision energy were performed manually on acteoside and its isomer isoacteoside standard solutions, and data acquisition in MRM mode was performed with Masslynx (v4.2). The transitions monitored were *m/z* 623.1 (CE 32 V) → *m/z* 161.1 (quantifier) and 461.1 at CE 28 V (qualifier) for acteoside and isoacteoside. A standard curve 8–5000 nM of both the analytes was run to test the linearity of the response and to confirm the different retention time of the two isomers. The accuracy of each standard point was calculated with TargetLynx based on the determined linear regression curve and should be between 80 % and 120 % of the expected value. Analyte quantity (acteoside + isoverbasoside) was extrapolated from the respective standard curves.

Cell viability assay

Cells viability was determined using the MTT (3-[4,5-dimethylthiazol-2-yl]-2,5 diphenyl tetrazolium bromide) assay. After treating cells for 72 h as described above, the culture medium was removed and cells were incubated for 2 h at 37 °C in 100 µL of DMEM containing 0.5 mg/mL MTT. Then, 100 µL of solubilization buffer (10 % Triton X-100, 0.1 N HCl in isopropanol) was added to cells. Absorbance was measured using a microplate reader (BioTek Synergy H1, Agilent) at 570 nm.

Analysis of reactive oxygen species (ROS) level in SH-SY5Y cells

Intracellular ROS were determined using fluorescent probe 2',7'-dichlorofluorescein diacetate, acetyl ester (H₂DCFDA, Merck). After treating cells for 72 h as described above, the culture medium was removed and cells were washed twice with PBS. Then, 5 µM of H₂DCFDA was added to each well for 30 min. After washing cells twice with PBS solution, the fluorescence was measured using a microplate reader (BioTek Synergy H1, Agilent) at excitation wavelength of 490 nm and emission wavelength of 520 nm. Data were normalized on total viability measured with MTT assay.

Western blot and native dot blot analyses

Cells were lysed in RIPA buffer (Thermo Scientific) supplemented with protease inhibitors (Roche) and phosphatase inhibitor cocktails (Merck). The lysates were centrifuged at 4 °C and the supernatants were collected. Protein concentration was determined using the Bradford assay (Bio-Rad). Protein samples were separated by SDS-PAGE and transferred to nitrocellulose membranes. After the transfer, the membranes were blocked with 5 % nonfat dry milk and primary antibodies anti-NRF2 (1:1000, ThermoFisher), anti-α-syn (Merck, 1:1000) and anti-vinculin (1:5000, Merck) were used. Conjugated secondary antibodies were applied, and the signal was detected using enhanced chemiluminescence (ECL). The resulting signals were captured using the Chemidoc system (Bio-Rad). For native dot blot analysis, samples from *in vitro* α-syn aggregation assays, performed in the absence or in the presence of the plant extracts, were dropped onto nitrocellulose membranes and incubated with the oligomer specific A11 mouse antibody (1:500, Thermo Fisher) or with the anti-α-syn antibody (1:1000, Merck).

Immunofluorescence assay

Cells grown on cover slips were washed with PBS, fixed with 4 % formaldehyde for 15 min, and permeabilized with PBS 0.2 % Triton X-100 for 10 min. Then, cells were washed in blocking solution (PBS 1 % BSA), blocked at room temperature for 60 min, and then incubated overnight at 4 °C with the primary antibody anti-α-Syn33 (1:40, Merck) recognizing α-syn oligomers, or with the primary antibody anti-NRF2 (1:200, Thermo Fisher). After that, cells were incubated with anti-rabbit AlexaFluor488 secondary antibodies (1:200, Thermo Fisher) for 1 h. Coverslips were mounted with a DAPI containing mounting medium for nuclear staining. Image acquisition was carried out on a Thunder fluorescence microscope (Leica Microsystems). For the analysis of α-syn oligomers, fluorescence images were analyzed using ImageJ software (NIH) and the Integrated Density (IntDen) of the α-syn fluorescence signal was quantified. Quantitative analysis of NRF2 nuclear localization was performed using Cell-ACDC, an open source user friendly GUI-based framework for segmentation [26]. Nuclei were segmented by applying an automated thresholding algorithm (Otsu method) on the DAPI channel, generating accurate nuclear masks. Within each segmented nucleus, the concentration parameter, defined as the total fluorescence intensity normalized to the nuclear area, was calculated. The resulting output data were exported and statistically analyzed to compare NRF2 localization across different treatment conditions.

Real time PCR

Total RNA was isolated using the Quick-RNA Mini-Prep Kit (Zymo Research), according to manufacturer's instructions. RNA (1 µg) was reverse-transcribed using iScript supermix (Bio-Rad), according to the manufacturer's protocol. For each real-time PCR, cDNA were amplified using the ChamQ mastermix (Vazyme) and specific primers. Each sample was normalized for total RNA content using ACTB and GAPDH as housekeeping genes. The primers used are the following: ACTB-F: CACCATTGGCAATGAGCGGT, ACTB-R: GTCTTTGCGGATGTCCACGT; GAPDH-F: AGAAGGCTGGGGCTCATTTG, GAPDH-R: TGCTAAGCAGTTGGTGGTGC; NQO1-F: TCCGGAGTAAGAAGGCAGTG, NQO1-R: TCCA GCGTTTCTCCATCC; HMOX1-F: TTCAAGCAGCTCTACCGCTC, HMOX1-R: TTGCACTTTGTTGCTGGCCC.

Size exclusion chromatography coupled to reversed phase LC-MS (SEC AS-MS)

For the SEC AS-MS analysis, the dry extracts were first diluted in 1 mL of dichloromethane (DCM) and dried under nitrogen to obtain the accurate weight. A 10 mg/mL solution in methanol was prepared and centrifuged for 5 min at 13,000 rpm and then diluted in water:methanol (70:30 v/v) to obtain a final concentration of 2 mg/mL. Incubation solutions (500 µL) containing 10 µM α-syn and the selected plant extracts (2 mg/mL) were prepared in 0.1 M potassium dihydrogen phosphate buffer at pH = 7 and incubated for 96 h at 4 °C. SEC AS-MS experiments of the incubated samples were carried out with two chromatographic systems (System 1 and System 2) as described in Ref. [15]. Briefly, System 1 was used for SEC analyses using a TSK Gel Super SW2000 125 Å column (300 × 4.6 mm ID, 4 µm) from Tosoh Bioscience. Analysis was carried out in isocratic elution (KH₂PO₄ 0.1 M, 0.05 % NaN₃, pH = 7) at a flow rate of 350 µL/min α-Syn was detected at λ = 280 nm and the peak was eluted in the window 6.5–8 min. The elution fraction (750 µL final volume) was focused on an Agilent Zorbax Eclipse Plus C18 analytical trap column (12.5 × 4.6 mm ID, 5 µm). The trap column was connected to System 2 on the head of an analytical column, an XTerra MS C18 column (250 × 2.1 mm ID, 5 µm) from Waters. Chromatographic separation of the plant extracts fished analytes and the analyses of the fingerprinting of the extracts were carried out through gradient elution where the mobile phase was water 0.1 % formic acid (solvent A) and acetonitrile 0.1 % formic acid (solvent B). Specifically, after an isocratic step at 1 % B for 11.50 min, a linear gradient of B from 1 % to 40 % was applied in 22 min. Then, three sequential linear gradient steps were performed (from 40 % to 70 % in 8.5 min, from 70 % to 90 % in 3.5 min and from 90 % to 100 % in 3.5 min). Lastly, an isocratic step was carried out at 100 % B for 8.5 min. Compound identification was achieved as reported in Ref. [15] through mass spectrometry (MS) using a linear ion trap mass spectrometer (LTQ) equipped with an electrospray ion source (ESI) (Thermo Fisher Scientific, Waltham, MA, USA). Full scan mass range was set up in the 250–1500 Da range.

Native mass spectrometry (Native-MS)

Native-MS analysis was performed to assess the interaction of α-syn with acteoside. Commercial α-syn (Merck Millipore) and acteoside (Merck) powders were individually resuspended in 100 mM ammonium acetate pH 7 at 1 mg/mL stock concentration. Titration experiments were performed preparing independent samples at fixed α-syn concentration (7 µM) and variable acteoside concentrations (0–1400 µM). Each sample (10 µL) was directly infused into the mass spectrometer (Orbitrap Fusion, Thermo Fisher Scientific) by a static nano-electrospray source, employing borosilicate, metal-coated capillaries with 1-µm internal diameter (Thermo Fisher Scientific). Analytes desolvation and charging were obtained applying a 1.1–1.2 kV ion spray voltage. The main instrumental parameters were set as follows: resolving power at m/z 200, 120,000; detection window, 700–2600 m/z ; IRM pressure, 3

mTorr (intact protein mode); ion-transfer tube temperature, 275 °C; in-source fragmentation, 0–5 V; AGC target, 4×10^5 ; maximum injection time, 100 ms. Tandem MS analysis at selected charge states of the protein-ligand complex was performed by collision-induced dissociation (CID) with helium gas. Final spectra were obtained by averaging the signal over 30 s acquisition. A ligand-binding curve was generated calculating the relative intensity ratio of bound vs. total α-syn peak signals.

Fly culture and acteoside treatment

DJ-1^{β^{ex54}} mutant flies (hereafter called *DJ-1*β) were used as PD model flies [27]. They were cultured on standard *Drosophila* food at 25 °C. For acteoside treatments, *DJ-1*β mutant second instar (L2) larvae were cultured on standard medium containing 0.1 % dimethyl sulfoxide (DMSO) (untreated flies) or supplemented with 250 or 400 µM acteoside (GenoChem World). After eclosion, adult female flies were transferred to new tubes and cultured for five days in vials containing DMSO or acteoside. Subsequently, flies were directly evaluated in climbing assays or frozen in liquid nitrogen and kept at –80 °C for quantification of protein carbonylation level. The effect of acteoside was also evaluated in flies treated only after eclosion: 1-day-old *DJ-1*β mutant female flies were transferred to new vials containing either 0.1 % DMSO (control) or acteoside-supplemented food (400 µM) and climbing assay was carried out 5 days and 10 days later.

Climbing assay and determination of carbonylation protein level

Locomotor performance of *DJ-1*β mutant flies was analyzed using climbing assay, which exploit flies' innate negative geotaxis, an upward movement response following mechanical stimulation. This simple, robust, and cost-effective behavioral test is widely used to evaluate motor function in fly models of neurodegenerative diseases [28]. In these assays, a total of 80–120 5-day-old female flies were analyzed per condition. Groups of 10–20 female flies were transferred to graduated plastic tubes (1.4 cm diameter), acclimated for 1 min, gently tapped down to the bottom and allowed to climb for 10 s, recording the process. Moreover, climbing assays were also carried out in 5-day-old and 10-day-old female flies treated only after eclosion. The climbing ability of untreated (DMSO) and acteoside-treated flies was determined as the average of the height reached by each fly after this time [29]. Protein carbonyl groups were measured in extracts from *DJ-1*β female flies of different ages and subjected to different treatment regimes using 2, 4-dinitrophenylhydrazine (DNPH) derivatization in 96-well plates (Greiner 96 well plate, polypropylene) as previously described [30].

Statistical analysis

All experiments were conducted in triplicate. Results are presented as mean ± standard deviation (SD). Statistical analyses were made using the two-tailed Student's t-test, with significance set at $p < 0.05$. For *Drosophila* experiments, groups were statistically compared by one-way ANOVA analysis followed by Tukey's post hoc test ($*p < 0.05$).

Results

Plant species selection

Within a collection of plant species belonging to the Italian flora, in the frame of the Italian initiative NBFC (National Biodiversity Future Center, <https://www.nbfc.it>), extracts from 60 plant species rich in specialized metabolites were selected and tested. While the chemical structures of primary metabolites are common across various species, specialized metabolites sharing core structures often exhibit a distribution linked to specific genetic lineages [31]. Thus, to facilitate a broad exploration of specialized metabolites with their bioactivities, species

from all major clades of Angiosperms were included in this investigation. The species, listed in [Supplementary Table S1](#), encompass monocots and eudicots, representing a total of 24 orders and 40 families. Additionally, two more primitive vascular species belonging to the Pteridophyta group were also included. Among the 60 analyzed species, the leaves of 11 plants (*Althaea officinalis*, *Aloysia citrodora*, *Artemisia abrotanum*, *Beta vulgaris*, *Castanea sativa*, *Diospyros kaki*, *Filipendula ulmaria*, *Lysimachia vulgaris*, *Rosa canina*, *Salvia pratensis*, *Verbascum thapsus*) are included in the Belfrit list, which defines a common reference for the use of plants in food supplements [32]. The inclusion of these species is particularly relevant, as it allows for a deeper evaluation of their specialized metabolites for public health applications [33].

To screen for the promising neuroprotective properties of this plant extract library, we conducted two complementary analyses: an *in silico* phylogenetic analysis to select potential medicinal plants, and a screening using a yeast model expressing the human protein α -syn, to select protective extracts against misfolded α -syn also in a cellular system.

Phylogenetic selection approach

Phylogenetic analyses identified 34, 45 and 50 hot trees related to antiaggregant, antiparkinsonian, and neuroprotective biological activities, respectively ([Supplementary Table S3](#)). The hot trees containing at least a taxa included in the list of 60 plants of NBFC project were plotted ([Supplementary Fig. S1](#)). All taxa included in hot trees were defined as Potential Medicinal Plants (PMP) if these were not already recognized as Medicinal Plants (MP) in the databases used. The plant species appearing in both the list of 60 plants and the hot trees are listed in [Table 1](#) specifying if these are MP or PMP. In [Fig. 1A](#) and [B](#) two examples of hot trees are plotted, wherein the clade encompassing the plant species identified by the phylogenetic approach applied in this study ([Table 1](#)) was enlarged for clarity. Altogether, our analysis identified 7 plants of our library associated with the antiaggregant biological function, 8 plants with the antiparkinsonian effect and 4 plants with the neuroprotective properties ([Table 1](#)). Therefore, a total of 11 plants (*Allium angulosum*, *Allium lusitanicum*, *Castanea sativa*, *Medicago marina*, *Salvia pratensis*, *Verbascum thapsus*, *Glaucium flavum*, *Acorus calamus*, *Althaea officinalis*, *Malva alcea*, *Artemisia abrotanum*), selected on the basis of the phylogenetic analysis ([Table 1](#)), have a high probability to present a medicinal value.

High-throughput screening of plant extracts with anti-aging and antioxidant effects

In parallel with the *in silico* analysis, a high-throughput screening on the 60 extracts of our library was conducted *in vivo* using a *S. cerevisiae* PD model, in which the human protein α -syn is overexpressed [34,35]. The Omnilog Biolog instrument was first employed to evaluate the effect of all plant extracts (at a concentration corresponding to 20 mg of fresh leaves/mL medium) on yeast cell growth. This step allowed us to exclude extracts exhibiting cytotoxicity, enabling a focused analysis of biologically relevant candidates to be considered in the following assays. Out of 60 plant extracts tested, only two obtained from *Heuchera sanguinea* and *Empetrum hermaphroditum*, showed relevant cellular toxicity and were thus excluded from further analysis ([Fig. 2A](#)). Of the other 58, 10 extracts did not significantly influence cell growth, while the remaining ones (48) stimulated the cell proliferation (expressed as maximal growth obtained after 72 h). On the basis of these data, we proceeded with a detailed analysis of the 58 non-toxic extracts in order to explore their potential anti-aging, antioxidant, and neuroprotective properties.

These 58 extracts were tested in the context of a standard chronological life span (CLS) experiment [36], to evaluate any ameliorating effect on the age-dependent α -syn mediated cell death, as we also recently reported [23]. Most extracts increased both mean and maximal

Table 1

Plant species appearing in both the list of 60 plants of NBFC-project and the hot trees subdivided for biological activity. In the category column: MP = Medicinal Plants, PMP = Potential Medicinal Plants.

Biological Activity	NBFC-project	Category
Antiaggregant	<i>Allium angulosum</i>	PMP
	<i>Allium lusitanicum</i>	PMP
	<i>Castanea sativa</i>	MP
	<i>Medicago marina</i>	PMP
	<i>Salvia pratensis</i>	PMP
	<i>Verbascum thapsus</i>	MP
	<i>Glaucium flavum</i>	MP
	<i>Acorus calamus</i>	MP
	<i>Allium angulosum</i>	PMP
	<i>Allium lusitanicum</i>	PMP
Antiparkinsonian	<i>Althaea officinalis</i>	MP
	<i>Castanea sativa</i>	MP
	<i>Malva alcea</i>	PMP
	<i>Artemisia abrotanum</i>	PMP
	<i>Salvia pratensis</i>	PMP
	<i>Allium angulosum</i>	PMP
	<i>Allium lusitanicum</i>	PMP
Neuroprotective	<i>Artemisia abrotanum</i>	PMP
	<i>Salvia pratensis</i>	PMP

lifespan of yeast cells (as indicated by the yellow color in the heatmap, [Fig. 2B](#)), except for those from *Glandularia tenera*, *Pseudosasa japonica* and *Acorus calamus*. Notably, 18 different extracts (*Echinophora spinosa*, *Acalypha virginica*, *Pulsatilla montana*, *Butomus umbellatus*, *Ranunculus lingua*, *Typha laxmannii*, *Centranthus ruber*, *Aquilegia atrata*, *Allium lusitanicum*, *Eryngium maritimum*, *Glaucium flavum*, *Verbascum thapsus*, *Succisa pratensis*, *Valeriana dioica*, *Salvia pratensis*, *Akebia quinata*, *Sternbergia lutea* and *Adenophora liliifolia*) exhibited very potent anti-aging activities, increasing mean lifespan more than 3.5 fold compared to the control condition. Coherently, these extracts also extended the maximum lifespan, although at different extents ([Fig. 2B](#)).

Alongside a decreased lifespan, oxidative stress is a typical feature of toxic protein aggregation induced by α -syn [37]; therefore the intracellular ROS level after 24 h treatment with the extracts were also quantified. Strikingly, 16 extracts (*Pulsatilla montana*, *Sternbergia lutea*, *Osyris alba*, *Rosa canina*, *Nonea lutea*, *Ranunculus lingua*, *Salvia pratensis*, *Malva alcea*, *Glaucium flavum*, *Succisa pratensis*, *Verbascum thapsus*, *Euonymus europaeus*, *Adenophora liliifolia*, *Allium lusitanicum*, *Inula salicina*, *Valeriana dioica*) decreased intracellular ROS level more than 2.5 fold ([Fig. 2B](#)). Therefore, 10 extracts showed the ability to attenuate both senescence and oxidative stress, two key hallmarks of age-related diseases ([Fig. 2C](#)), they derived from *Ranunculus lingua*, *Verbascum thapsus*, *Adenophora liliifolia*, *Valeriana dioica*, *Allium lusitanicum*, *Succisa pratensis*, *Salvia pratensis*, *Pulsatilla montana*, *Glaucium flavum* and *Sternbergia lutea*. These plants belong to different plant families but, with the exception of *Allium lusitanicum* that contains only saponins, the other plant extracts share some chemical similarities as eight species are characterized by the presence of flavonoids. Specifically, *Adenophora liliifolia*, *Ranunculus lingua*, *Succisa pratensis* and *Verbascum thapsus* have compounds belonging to the flavone class (*e.i.* luteolin and derivatives), while *Glaucium flavum*, *Pulsatilla montana*, *Sternbergia lutea* and *Valeriana dioica* have compounds belonging to the flavanol class (*e.i.* quercetin and derivatives). Furthermore, six of these ten plant extracts with antiaging and antioxidant activity (*Glaucium flavum*, *Pulsatilla montana*, *Ranunculus lingua*, *Salvia pratensis*, *Succisa pratensis* and *Valeriana dioica*) are characterized by the presence of compounds from the cinnamyl derivative class, known for their antioxidant properties [38].

From the combination of the three screening methods, *i.e.* phylogenetic identification as a medicinal plant, increase of mean lifespan (>3.5 fold) and decrease of ROS level (>2.5 fold), we identified 4 plant extracts responding to all three criteria ([Fig. 2C](#)). In fact, from the phylogenetic analysis, 11 species were identified as potential medicinal plants

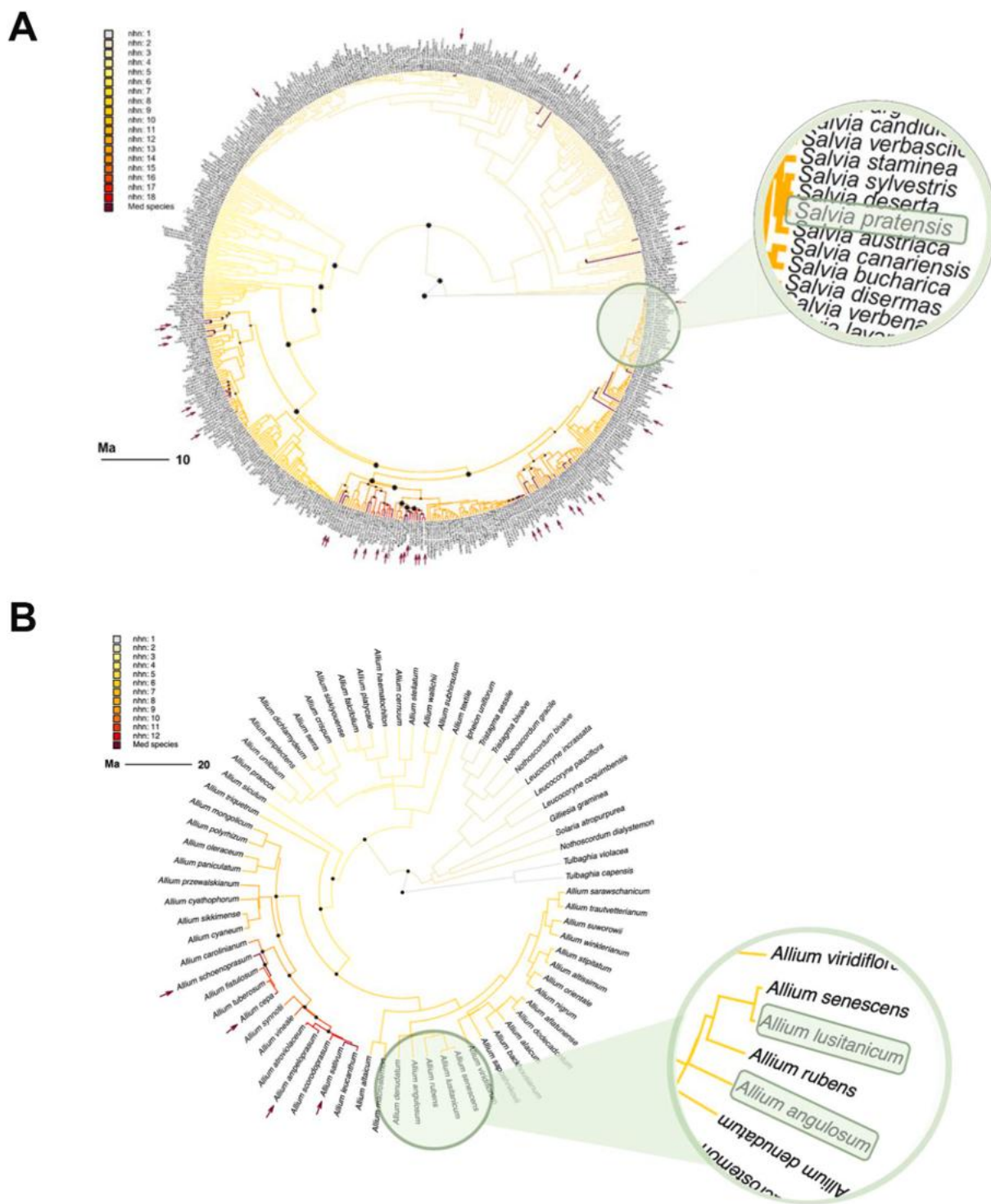
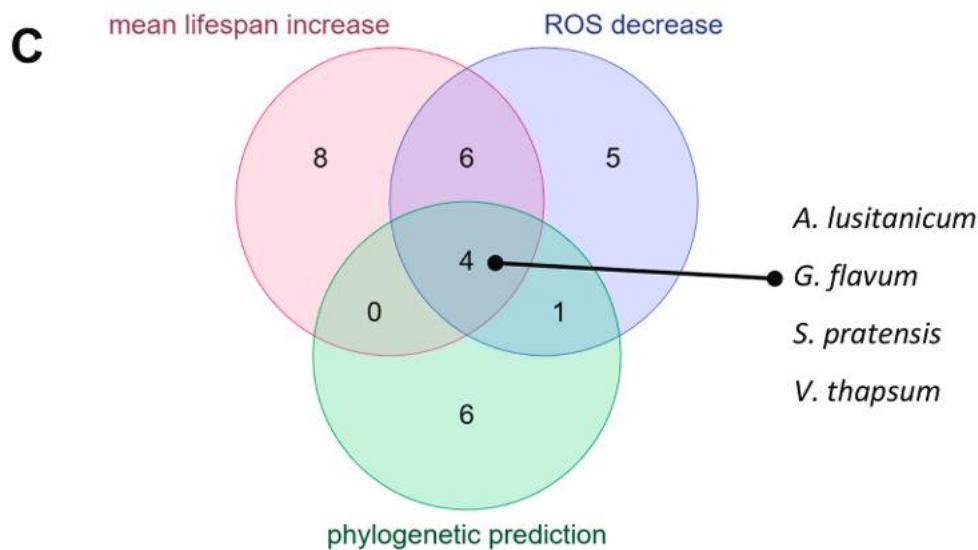
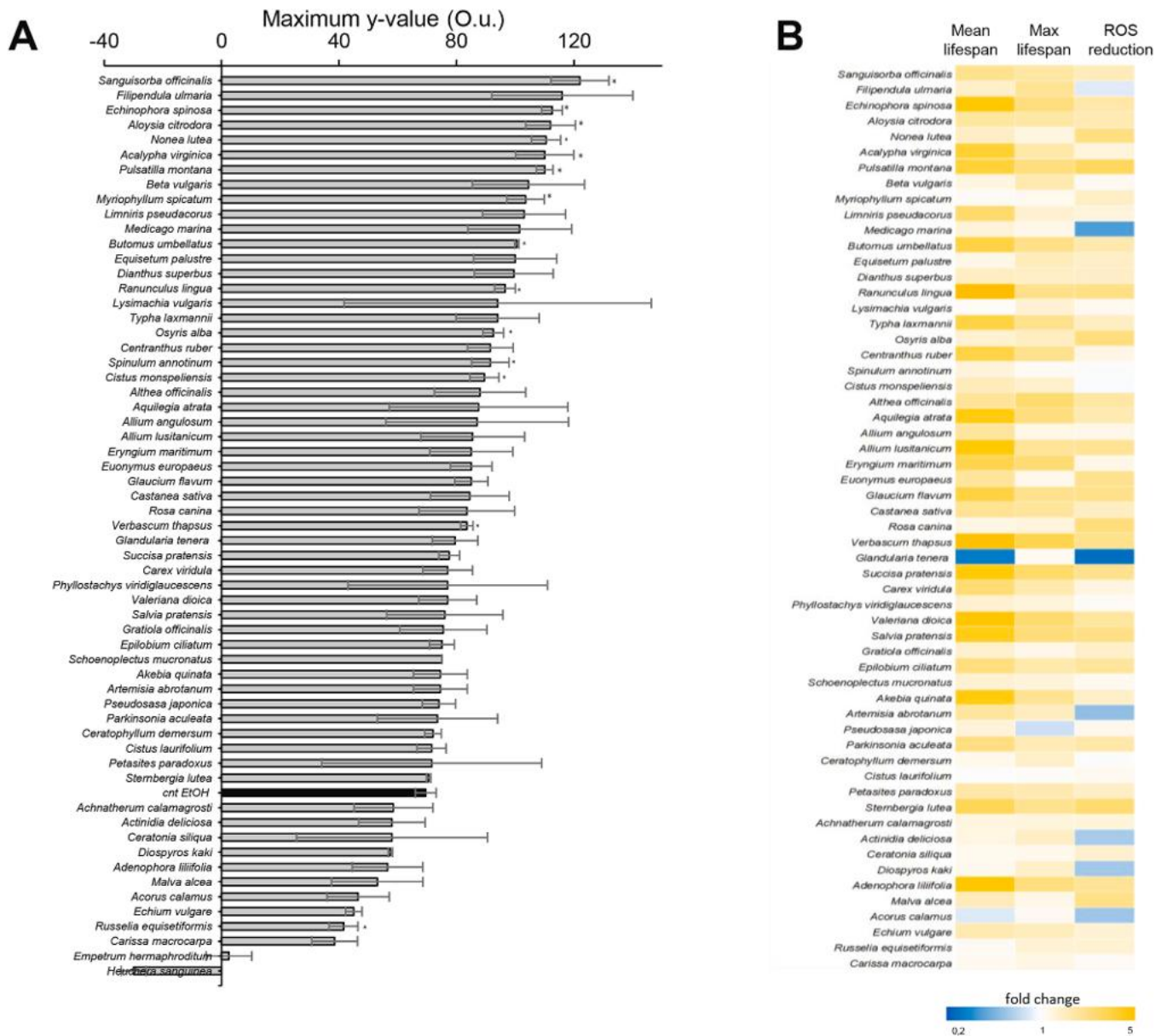


Fig. 1. Phylogenetic analysis. Phylogenetic hot tree associated with neuroprotective (A) and antiaggregant (B) biological activity. The branch colors increase from white to red proportionally to the number of nested hot nodes (nhn). Medicinal Plants (MP) are indicated by an arrow and their branches are highlighted in purple. All hot nodes are indicated with a black circle. Horizontal bar giving the scale of the branch lengths in million years (Ma).

(PMP) or medicinal plants (MP) (Table 1), but only 4 of them, *A. lusitanicum*, *G. flavum*, *S. pratensis* and *V. thapsus*, were also able to improve cell longevity (>3.5 fold increase) and reduce intracellular ROS (>2.5 fold decrease) in the yeast model (Fig. 2C). Consequently, the combination of these approaches underscores the potential preventive and therapeutic benefits of *A. lusitanicum*, *G. flavum*, *S. pratensis* and *V. thapsus* against neurodegenerative diseases such as Parkinson’s disease.

Phytochemical profiles of A. lusitanicum, G. flavum, S. pratensis and V. thapsus extracts

Building on the promising biological findings, the phytochemical profiles of the above selected species were obtained and shown in Fig. 3 as base peak chromatograms recorded in negative ionization (only for *G. flavum* we reported also the positive ionization chromatogram to highlight the exclusive occurrence of alkaloids). The four species are characterized by



(caption on next page)

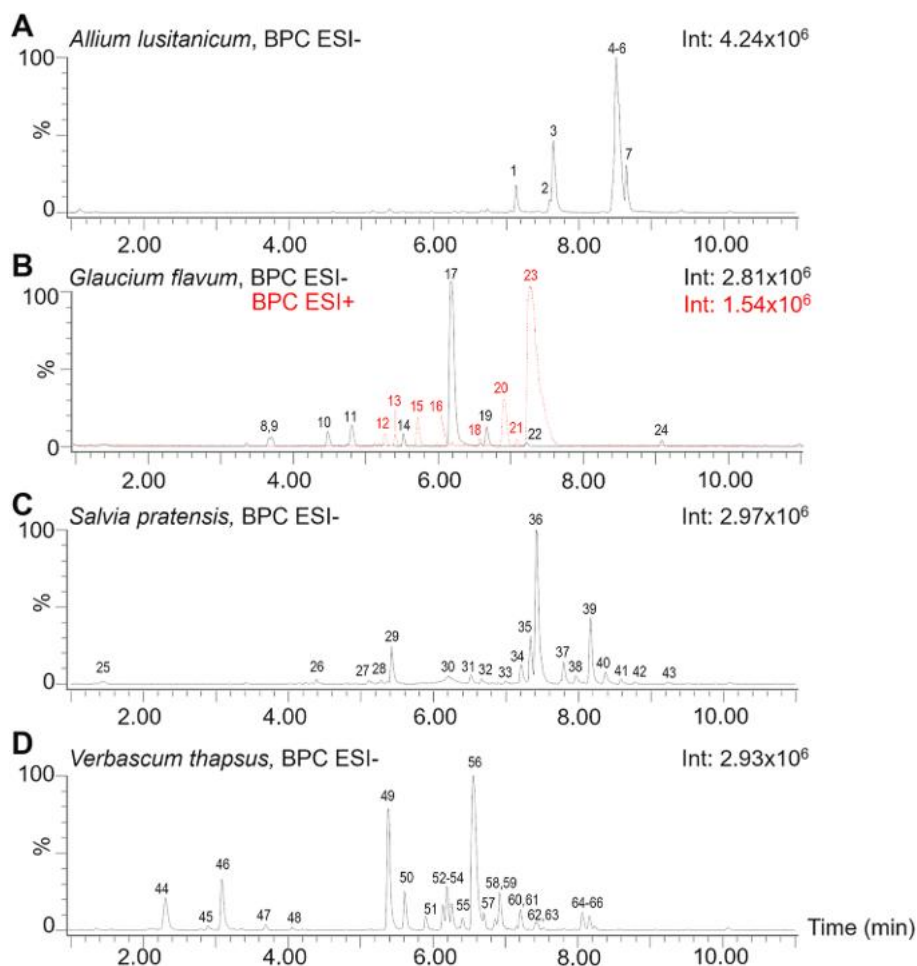


Fig. 3. Specialized metabolite-profiling of the selected plant extracts. Base peak chromatograms, in negative ionization mode, of *Allium lusitanicum* (A), *Glaucium flavum* (B), *Salvia pratensis* (C) and *Verbascum thapsus* (D). For *G. flavum* also the positive ionization chromatogram is shown in red. The ID of the peaks are the same as Table 2.

the presence of different classes of secondary metabolites, their identity and LC-MS features are reported in Table 2. *A. lusitanicum* accumulates different glycosides of steroidal saponins characterized by furostane, spirostane and cholestane skeletons (Fig. 3A, Table 2). A more exhaustive phytochemical characterization of this species is reported in a previous published work [15]. *G. flavum* is characterized by the accumulation of large amounts of glaucine and other aporphine/isoquinoline alkaloids, while rutin is the most abundant flavonoid among the polyphenols detected (Fig. 3B, Table 2). *S. pratensis* accumulates a wide array of polyphenols, mainly rosmarinic acid and its derivatives as well as other caffeic acid esters such as salvianolic acids (Fig. 3C, Table 2). *V. thapsus* presents a more diversified profile with the occurrence of iridoid glucosides (mainly catalpol) and their derivatives esterified to various hydroxycinnamic acids; moreover, this species presents large amounts of acteoside (Supplementary Fig. S2) and minor amounts of acteoside isomers and other phenylpropanoid/phenylethanoid glycosidic esters (such as leucosceptoside and martynoside) (Fig. 3D, Table 2).

The extracts of S. pratensis, V. thapsus and G. flavum inhibit α -syn aggregation

Recent studies indicate that a number of natural extracts can display a direct inhibition of amyloid fibril formation [6,39]. These findings have spurred interest in exploring plant-derived compounds as potential therapeutic agents targeting protein misfolding and aggregation.

To investigate these promising features, the anti-aggregant properties of the four selected extracts, *A. lusitanicum*, *S. pratensis*, *V. thapsus* and *G. flavum* were evaluated through a multi-tiered approach, that integrates complementary systems, including yeast cultures and neuroblastoma cells expressing human α -syn, as well as direct protein interaction studies. This multifaceted strategy allowed us to explore their effects at various biological levels, ranging from cellular outputs to direct molecular interactions.

Firstly, we investigated whether the positive effects of the extracts on yeast longevity (Fig. 4A–C), also reported in the heatmap of Fig. 2B,

Fig. 2. Screening in yeast cells. (A) Effect of the extracts on cell growth: maximum y-value of growth kinetics of yeast cells overexpressing α -syn, grown in minimal medium containing 2 % glucose for 72 h in the absence (cnt) or presence of the extracts (corresponding to 20 mg fresh leaves/mL medium). The black bar identifies the control (cnt). * $p < 0.05$ relative to maximum y-value in control cells ($n = 3$). (B) Heatmap showing the effect of the plant extracts on mean lifespan, maximal lifespan and ROS reduction on yeast cells overexpressing α -syn. Data are expressed as fold change compared to control condition and are visualized using a color scale, with yellow indicating an increase and blue indicating a decrease of each parameter ($n = 3$). (C) Venn diagram of the plant extracts resulting from the phylogenetic analysis and the screening in yeast cells. The increase of mean lifespan of at least 3.5 fold and the reduction of ROS level of at least 2.5 fold have been considered. The extracts from *A. lusitanicum*, *S. pratensis*, *V. thapsus* and *G. flavum* have been selected by all three screening systems.

Table 2

LC-MS features of the main specialized metabolites detected in the extracts of *Allium lusitanicum*, *Glaucium flavum*, *Salvia pratensis* and *Verbascum thapsus*. Peak IDs refer to peak numbers of Fig. 3. Abbreviations: FA, formic acid; Rt, retention time; UI, unidentified.

Peak ID	Compound	Rt (min)	Molecular formula	Precursor ion	<i>m/z</i> observed	Error (ppm)	Diagnostic product ions (<i>m/z</i>)	MSI level ^a
<i>Allium lusitanicum</i>								
1	Saponin class IV4 + 2 hexoses + desoxyhexose	7.13	C ₄₅ H ₇₄ O ₁₉	[M + FA-H] ⁻	963.481	-1.45	447.312; 609.364; 771.423; 917.480	2
2	Saponin class IV4 + 2						hexoses + desoxyhexose + acetyl group 447.312; 609.364; 771.423; 917.480	7.60 2
3	Saponin class IV4 + 2		C ₄₇ H ₇₆ O ₂₀	[M + FA-H] ⁻	1005.492	-1.99	hexoses + desoxyhexose + acetyl group 447.311; 609.364; 771.423; 899.468; 917.477; 959.485	7.65 2
4	Saponin class IV3 + 2 hexoses + 2 desoxyhexoses	8.46	C ₅₁ H ₈₄ O ₂₂	[M + FA-H] ⁻	1093.545	-1.55	431.319; 593.369; 755.426; 901.482; 1047.541	2
5	Saponin class IV3 + 2 hexoses + 3 desoxyhexoses	8.51	C ₅₇ H ₉₄ O ₂₆	[M - H] ⁻	1193.598	-2.51	431.315; 575.356; 593.369; 755.420; 883.470; 901.482; 1047.541	2
6	Saponin class IV3 + 2		C ₅₀ H ₈₂ O ₂₂	[M + FA-H] ⁻	1079.531	-3.71	hexoses + desoxyhexose + pentose 431.319; 593.369; 755.426; 901.482	8.55 2
7	Saponin class IV3 + 2 hexoses + desoxyhexose	8.65	C ₄₅ H ₇₄ O ₁₈	[M + FA-H] ⁻	947.487	-1.79	431.315; 593.374; 755.426; 901.482	2
<i>Glaucium flavum</i>								
8	Vanillyl alcohol hexoside isomer 1	3.71	C ₁₄ H ₂₀ O ₈	[M - H] ⁻	315.108	-0.04		2
9	Vanillyl alcohol hexoside isomer 2	3.75	C ₁₄ H ₂₀ O ₈	[M - H] ⁻	315.108	-0.04	153.056; 135.046	2
10	Coumaroyl quinic acid	4.52	C ₁₆ H ₁₈ O ₈	[M - H] ⁻	337.0923	0.11	191.057; 163.041; 119.050	2
11	Feruloyl quinic acid	4.87	C ₁₇ H ₂₀ O ₉	[M - H] ⁻	367.1029	0.01	193.051; 149.061; 134.037	2
12	Laurifoline	5.27	C ₂₀ H ₂₄ NO ₄ ⁺	[M] ⁺	342.1705	0.07	297.114; 282.087; 265.087; 237.090; 222.070; 219.080; 207.080; 191.085; 165.072	2
13	Isoboldine/Salutaridine isomer	5.44	C ₁₉ H ₂₁ NO ₄	[M+H] ⁺	328.1549	-0.08	297.110; 285.12; 265.084; 239.069; 237.093; 192.101	2
14	Caffeoyl malic acid	5.57	C ₁₃ H ₁₂ O ₈	[M - H] ⁻	295.0454	-0.03	179.033; 135.046; 133.015; 115.003	2
15	Isoboldine or Salutaridine isomer 3	5.78	C ₁₉ H ₂₁ NO ₄	[M+H] ⁺	328.1549	-0.08	297.114; 265.087; 237.090; 233.060; 222.069; 205.066; 194.071; 177.069	2
16	Corydine/Isocorydine isomer	6.14	C ₂₀ H ₂₃ NO ₄	[M+H] ⁺	342.1689	4.75	236.083; 265.084	2
17	Rutin	6.17	C ₂₇ H ₃₀ O ₁₆	[M - H] ⁻	609.1456	-0.08	300.026; 271.026; 255.031	1
18	Corydine/Isocorydine isomer	6.61	C ₂₀ H ₂₃ NO ₄	[M+H] ⁺	342.1705	0.07	311.129; 279.095; 251.106; 236.083	2
19	Kaempferol hexose-deoxyhexose	6.70	C ₂₇ H ₃₀ O ₁₅	[M - H] ⁻	593.1506	0.06	285.041; 255.031; 227.035	2
20	Protopine	6.86	C ₂₀ H ₁₉ NO ₅	[M+H] ⁺	354.1341	0.12	336.121; 275.068; 247.073; 206.080; 188.071; 149.059	2
21	Norchelidonine	7.09	C ₁₉ H ₁₇ NO ₅	[M+H] ⁺	340.1164	6.15	275.068; 189.069; 247.077; 305.079; 323.091	2
22	UI	7.24	C ₂₀ H ₃₀ O ₁₀	[M - H] ⁻	429.1761	-0.09	249.113; 205.124; 179.052; 161.133; 119.039	2
23	Glaucine	7.26	C ₂₁ H ₂₅ NO ₄	[M+H] ⁺	356.1862	-0.07	325.142; 310.119; 294.128; 279.099; 251.106; 236.083	2
24	3β,23-dihydroxy-30-norolean-12,20-dien-28-oic acid hexose-hexuronic acid	9.08	C ₄₁ H ₆₂ O ₁₅	[M - H] ⁻	793.401	0.03	631.352; 455.312	2
<i>Salvia pratensis</i>								
25	UI	1.44	C ₁₀ H ₆ O ₈	[M - H] ⁻	252.9984	0.17	136.985; 116.928; 115.002; 71.008	2
26	Caffeoyl threonic acid	4.39	C ₁₃ H ₁₄ O ₈	[M - H] ⁻	297.0629	-6.26	179.036; 161.029; 135.030; 117.017; 75.006	2
27	C ₉ H ₁₂ O ₃ -hexose-deoxyhexose	5.11	C ₂₁ H ₃₂ O ₁₂	[M + FA-H] ⁻	521.1863	1.38	475.184; 113.024; 329.124; 161.047; 149.061; 311.113; 167.074	3
28	Tuberonic acid hexoside	5.28	C ₁₈ H ₂₈ O ₉	[M - H] ⁻	387.1664	-2.33	207.103; 163.113	2
29	Rosmarinic acid hydrate	5.42	C ₁₈ H ₁₈ O ₉	[M - H] ⁻	377.0873	-0.12	359.0787; 197.0464; 179.0338; 161.0261; 135.0465; 133.0301	2
30	Salvianolic acid A	6.17	C ₂₆ H ₂₂ O ₁₀	[M - H] ⁻	493.1135	-0.07	313.0726; 295.0627; 185.0256; 109.0307	2
31	Luteolin-O-hexoside	6.51	C ₂₁ H ₂₀ O ₁₁	[M - H] ⁻	447.0943	-3.51	285.038	2
32	Rosmarinic acid hexose	6.70	C ₂₄ H ₂₆ O ₁₃	[M - H] ⁻	521.1287	1.55	359.075; 341.086; 323.077; 197.046; 179.034; 161.023; 135.044	2
33	Sagerinic acid	6.99	C ₃₆ H ₃₂ O ₁₆	[M - H] ⁻	719.1615	-0.41	161.026; 359.075; 197.044; 179.036; 341.067; 135.044	2
34	Luteolin acetylhexoside	7.19	C ₂₃ H ₂₂ O ₁₂	[M - H] ⁻	489.1029	0.81	447.090; 285.042	2
35	Salvianolic acid K	7.34	C ₂₇ H ₂₄ O ₁₃	[M - H] ⁻	555.1139	-0.07	493.115; 359.079; 295.059; 197.046; 179.034; 161.026; 135.046	2
36	Rosmarinic acid	7.41	C ₁₈ H ₁₆ O ₈	[M - H] ⁻	359.0767	-0.03	197.046; 179.036; 161.026; 135.046; 133.030; 123.046	1

(continued on next page)

Table 2 (continued)

Peak ID	Compound	Rt (min)	Molecular formula	Precursor ion	<i>m/z</i> observed	Error (ppm)	Diagnostic product ions (<i>m/z</i>)	MSI level ^a
37	Lithospermic acid	7.77	C ₂₇ H ₂₂ O ₁₂	[M – H] [–]	537.1033	–0.01	493.115; 359.079; 295.059; 221.044; 197.046; 179.036; 161.023; 135.044; 133.030	2
38	Chrysoeriol-(3-Hydroxy-3-methylglutaryl)-O-hexoside	7.96	C ₂₈ H ₃₀ O ₁₅	[M – H] [–]	605.1477	4.86	503.119; 461.107; 299.056; 284.034; 255.030	2
39	Octene alcohol-hexose-pentose	8.15	C ₁₉ H ₃₄ O ₁₀	[M + FA-H] ⁺	467.2129	–0.13	421.208; 289.169; 161.044; 149.046; 131.033; 113.024; 101.022	2
40	Methyl rosmarinatate	8.37	C ₁₉ H ₁₈ O ₈	[M – H] [–]	373.0923	0.10	197.046; 179.036; 175.039; 160.017; 135.044; 123.046	2
41	UI	8.58	C ₂₈ H ₂₈ O ₁₅	[M – H] [–]	603.1355	–0.85	317.065; 137.025; 197.044; 87.008; 93.032	2
42	UI	8.77	C ₂₁ H ₃₆ O ₁₀	[M + FA-H] ⁺	493.2289	–0.83	447.224; 315.180; 161.047; 359.083	2
43	Salvianolic acid L	9.23	C ₃₆ H ₃₀ O ₁₆	[M – H] [–]	717.1456	–0.06	519.095; 338.052; 179.034; 161.023; 135.044	2
<i>Verbascum thapsus</i>								
44	Catalpol	2.30	C ₁₅ H ₂₂ O ₁₀	[M + FA-H] ⁺	407.1192	–0.62	199.061; 169.052; 181.052; 151.040; 163.039; 137.025	2
45	UI	2.89	C ₂₁ H ₃₂ O ₁₄	[M + FA-H] ⁺	553.1761	1.36	507.176; 345.121; 181.049; 315.103; 163.041; 151.039; 231.088; 327.111	2
46	Aucubin	3.08	C ₁₅ H ₂₂ O ₉	[M + FA-H] ⁺	391.124	1.10	345.121; 179.053; 183.065; 165.054	2
47	Dihydroaucubin	3.69	C ₁₅ H ₂₄ O ₉	[M + FA-H] ⁺	393.142	–5.90	347.131; 185.081; 179.055; 167.072	3
48	Forsythoside	4.05	C ₂₀ H ₃₀ O ₁₂	[M – H] [–]	461.165	1.94	135.046; 113.025; 315.110; 297.100; 161.045	2
49	Hydroxy-saccatoside (Catalpol-O-caffeoyl-deoxyhexoside) isomer 1	5.39	C ₃₀ H ₃₈ O ₁₇	[M – H] [–]	669.205	–2.59	161.025; 133.029; 163.039; 179.033; 135.044	3
50	Hydroxy-saccatoside (Catalpol-O-caffeoyl-deoxyhexoside) isomer 2	5.61	C ₃₀ H ₃₈ O ₁₇	[M – H] [–]	669.205	–2.59	161.025; 133.029; 163.039; 179.033; 135.044	3
51	Saccatoside (Catalpol-O-coumaroyl-deoxyhexoside)	5.9	C ₃₀ H ₃₈ O ₁₆	[M – H] [–]	653.205	4.21	145.031; 377.124; 163.041; 491.157; 291.087; 117.035	3
52	Methoxy-saccatoside (Catalpol-O-feruloyl-deoxyhexoside)	6.14	C ₃₁ H ₄₀ O ₁₇	[M – H] [–]	683.219	–0.13	175.041; 160.016; 407.136; 193.051	3
53	Acteoside-pentose	6.19	C ₃₄ H ₄₄ O ₁₉	[M – H] [–]	755.241	–1.93	593.210; 161.025; 133.029; 447.151; 179.033; 135.046; 125.025	2
54	Apigenin-hexose-hexuronide	6.27	C ₂₇ H ₂₈ O ₁₆	[M – H] [–]	607.130	0.17	269.046; 431.102; 225.057	2
55	Verminoside (caffeoyl-catalpol)	6.41	C ₂₄ H ₂₈ O ₁₃	[M – H] [–]	523.147	–2.95	161.025; 179.033; 135.046; 133.029	2
56	Acteoside	6.56	C ₂₉ H ₃₆ O ₁₅	[M – H] [–]	623.197	1.58	161.025; 461.165; 133.029; 179.036; 135.046; 113.025	1
57	Leucosceptoside A-pentose	6.70	C ₃₅ H ₄₆ O ₁₉	[M – H] [–]	769.256	–0.01	593.210; 175.041; 160.016; 193.051; 447.151;	2
58	Acteoside isomer 1	6.86	C ₂₉ H ₃₆ O ₁₅	[M – H] [–]	623.197	1.42	161.025; 461.165; 133.029; 179.036; 135.046; 113.025	2
59	Acteoside isomer 2	6.92	C ₂₉ H ₃₆ O ₁₅	[M – H] [–]	623.197	1.42	161.025; 461.165; 133.029; 179.036; 135.046; 113.025	2
60	Scutellarioside II (p-coumaroyl-catalpol)	7.16	C ₂₄ H ₂₈ O ₁₂	[M – H] [–]	507.153	–4.45	145.028; 231.066; 345.098; 163.041; 119.050	2
61	Leucosceptoside A	7.21	C ₃₀ H ₃₈ O ₁₅	[M – H] [–]	637.214	–0.42	461.165; 175.041; 160.016; 193.051; 135.046; 113.025	2
62	Martynoside-pentose	7.41	C ₃₆ H ₄₈ O ₁₉	[M – H] [–]	783.273	–1.73	175.041; 607.226; 193.051; 160.016; 461.169	2
63	Leucosceptoside A isomer	7.43	C ₃₀ H ₃₈ O ₁₅	[M – H] [–]	637.214	–0.42	461.165; 175.041; 160.016; 193.051; 135.046; 113.025	2
64	Martynoside	8.07	C ₃₁ H ₄₀ O ₁₅	[M + FA-H] ⁺	697.237	–4.21	651.230; 175.041; 160.016; 193.051; 475.182	2
65	Octene alcohol-hexose-pentose	8.15	C ₁₉ H ₃₄ O ₁₀	[M + FA-H] ⁺	467.211	4.15	289.166; 421.206; 161.048; 101.025; 113.025	3
66	Martynoside isomer	8.23	C ₃₁ H ₄₀ O ₁₅	[M – H] [–]	651.230	–0.95	175.041; 160.016; 193.051; 475.182	2

^a According to metabolomics standards initiative (MSI).

could be associated with their influence on the formation of intracellular aggresomes. It is widely recognized that these inclusion bodies of aggregated, misfolded proteins can arise in response to different cellular stress. Their abundance increases during the stationary phase and is markedly elevated in cells overexpressing α -synuclein (Supplementary Fig. S3, [24]); indeed they represent a typical hallmark of PD and other neurodegenerative diseases [40]. Notably, treatment with all four extracts resulted in a reduction of intracellular aggresomes, albeit to varying extents, ranging from 40 % (*G. flavum*) to a stronger reduction of

60 % (*A. lusitanicum* and *V. thapsus*) and 80 % (*S. pratensis*) (Fig. 4D). To further evaluate the ability of the selected extracts to prevent protein misfolding, SH-SY5Y neuroblastoma cell cultures conditionally expressing α -syn were also used [41]. Cells were treated with doxycycline to induce the overexpression of α -syn in the presence of the extracts, and the toxic oligomeric species of α -syn were detected following 48 h treatment. Notably, a significant decrease in α -syn oligomers was observed with *S. pratensis*, *V. thapsus*, and *G. flavum* extracts (around 40 %) (Fig. 5A–B), which also slightly affected cell viability

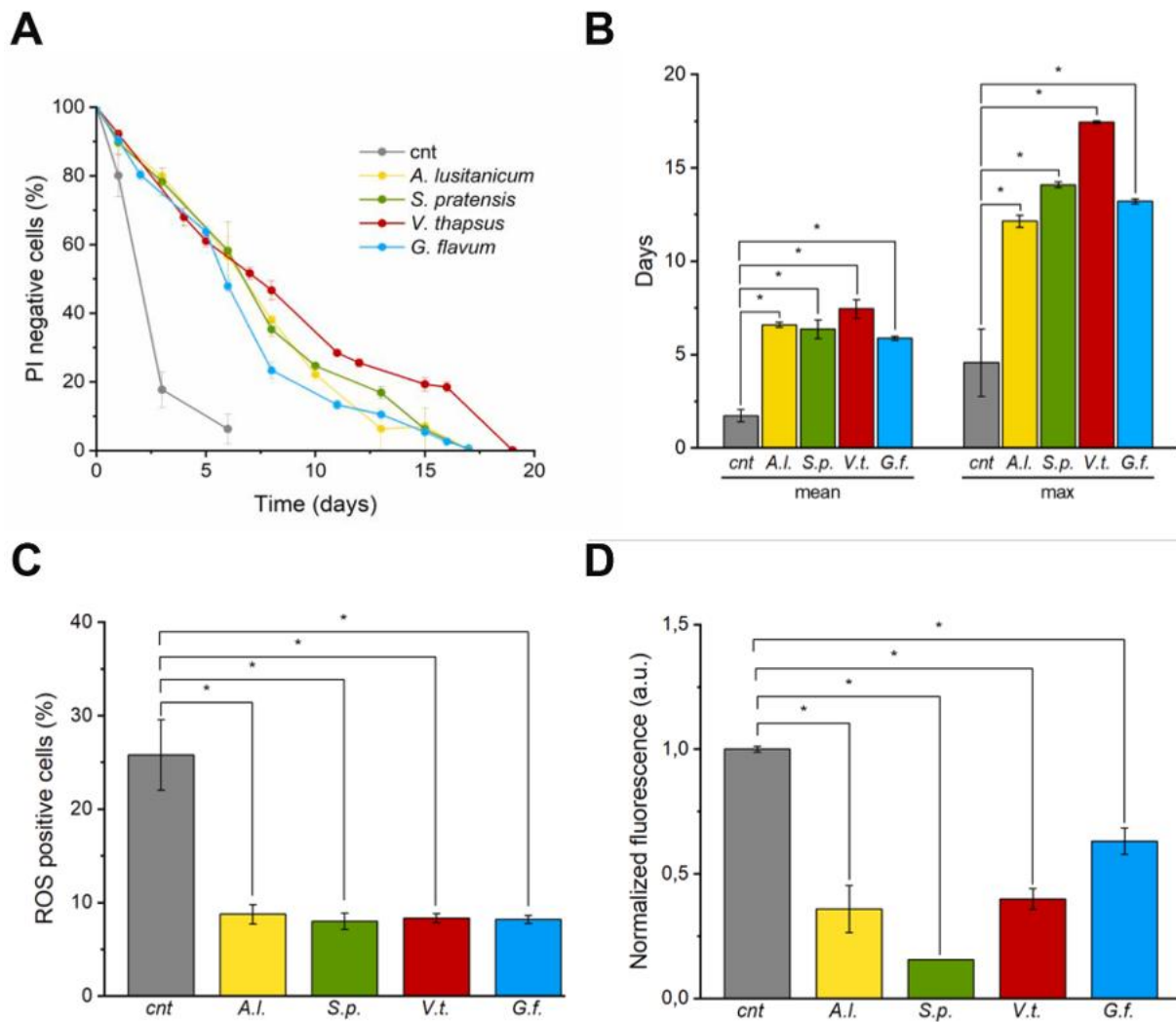


Fig. 4. The extracts from *A. lusitanicum*, *S. pratensis*, *V. thapsus* and *G. flavum* extend yeast lifespan. (A) CLS of yeast cells overexpressing α -syn grown in medium containing 2 % glucose in the absence or presence of *A. lusitanicum*, *S. pratensis*, *V. thapsus* and *G. flavum* extracts (at a concentration corresponding to 20 mg of fresh leaves/mL medium), added in exponential phase of growth. (B) Mean and maximal lifespan of cells in (A). (C) ROS content of cells treated for 24 h as in (A). (D) Aggregates level of cells treated for 24 h as in (A). Histograms represent mean \pm SD of at least three independent experiments. * $p < 0.05$.

(Supplementary Fig. S4A). Despite the difference in oligomeric forms, the total level of α -syn (both endogenous and overexpressed, which bears a FLAG-tag that enables to discriminate it from the endogenous protein) did not vary significantly with the treatments (Fig. 5C). In contrast, the extract from *A. lusitanicum*, which strongly reduced cell viability (Supplementary Fig. S4A), did not lower α -syn oligomer level at all (Fig. 5A–B). We speculate that its toxicity could overcome the potential activity of other beneficial compounds within the extract. Alternatively, these active molecules exhibited very low permeability, resulting in no detectable positive effect on cells.

Considering these results, we next investigated whether the extracts could inhibit the aggregation of the purified α -syn protein. To this end, we took advantage of the Thioflavin T (ThT) fibrillation assays to monitor α -syn aggregation over 72 h. In the absence of the extracts, ThT fluorescence exhibited a strong increase, indicating substantial amyloid fibril formation (Fig. 5D), as already known [25,42]. Strikingly, the presence of the extracts completely abolished this signal, with residual ThT fluorescence level of less than 2 % for *A. lusitanicum* and *G. flavum*, and 9 % and 17 % for *V. thapsus* and *S. pratensis*, respectively (Fig. 5D). The inhibition of fibril formation was also confirmed with a dot blot using A11 antibody, which specifically recognizes oligomeric α -syn

(Fig. 5E) and by TEM analysis (Fig. 5F). The results obtained strongly highlight that all the four extracts inhibit the aggregation of the purified α -syn protein *in vitro*.

Then, surface plasmon resonance (SPR) analysis was employed to assess direct interactions between the extracts and α -syn protein by immobilizing the protein on a CM5 sensor chip (as previously reported in Ref. [23]). The anti- α -syn antibody bound to the protein on the chip, whereas the oligomer-specific anti-Syn33 antibody did not (Supplementary Fig. S5A), confirming that the immobilized α -syn was in its monomeric form. This system was then used to test direct interactions between α -syn and the extracts from *A. lusitanicum*, *S. pratensis*, *V. thapsus*, and *G. flavum*. All extracts showed concentration-dependent binding to α -syn, with increasing extract concentrations producing higher SPR signals (Supplementary Fig. S5B–I). These results, along with previous ones, suggest that the extracts contain compounds that directly bind α -syn and inhibit its amyloid aggregation.

In conclusion, integrating data from yeast, neuroblastoma cells, and SPR analysis, extracts from *S. pratensis*, *V. thapsus*, and *G. flavum* consistently inhibited the formation of toxic α -syn oligomers across all models, indicating the presence of anti-aggregant compounds.

Acteoside from *V. thapsus* binds α -syn

In order to identify which metabolites present in the extracts can directly bind to α -syn protein, the extracts from *A. lusitanicum*, *S. pratensis*, *V. thapsus* and *G. flavum* were analyzed by size exclusion chromatography coupled to reversed phase LC-MS (SEC AS-MS). We decided to make this analysis considering all the extracts because the one from *A. lusitanicum* was able to affect α -syn aggregation *in vitro* (Fig. 5D–F), despite its inconsistent effect on neuroblastoma cells (Fig. 5A–B). An already established ligand fishing assay, based on size exclusion chromatography coupled to reversed phase LC-MS for the analysis of botanical extracts, was modified for the affinity screening of the four extracts toward α -syn [15].

Each extract was incubated with α -syn and injected in the SEC column to isolate and collect α -syn complexes. Bound ligands were desorbed from the trap column and analyzed by RPLC-MS. The LC-MS chromatograms of *G. flavum* and *S. pratensis* extracts obtained by the described fishing method did not reveal the presence of any bound ligands. As concerns the *A. lusitanicum* extract, we observed the fishing of 3 different saponins, putatively identified through the classification of the aglycone class and the number and type of sugars attached to it, in accordance with Geng et al. 2021 [43]: saponin class IV3 +2 hexoses +3 desoxyhexoses, saponin class IV3 +2 hexoses +1 desoxyhexose +1 pentose, saponin class IV3 +2 hexoses +1 desoxyhexoses (Supplementary Fig. S6A–C).

Notably, in the case of *V. thapsus* extract, the most abundant metabolite acteoside was successfully fished as reported in Fig. 6A. In particular, the chromatogram shows two peaks at retention times 27.35 and 28.20 corresponding to both isoforms of the molecule, able to bind α -syn (Fig. 6A, lower panel). These peaks correspond to acteoside and its isomer, and were identified by extracting the ionic current in the mass spectrum. Their presence was confirmed through fingerprinting and by comparing their mass values with those of the main molecules in the extract, as reported in Table 2. In the non-treated extract, they appeared at retention times 27.25 and 28.09 (Fig. 6A, upper panel), while in the SEC-AS-MS analysis of the incubated extract with α -syn, they shift slightly to 27.35 and 28.20. Interestingly, in the *V. thapsus* extract there are different structurally related compounds, such as leucosceptoside (phenylethanoid glycosides) or verminoside (caffeoyl-catalpol), but only acteoside was able to bind α -syn in the SEC AS-MS analysis, supporting the specificity of this binding.

Then, our analysis highlights that saponins from the extract of *A. lusitanicum* and acteoside from *V. thapsus* were able to bind α -syn protein. Interestingly, the abundance of the fished metabolites was always lower in the incubated samples compared to the extracts, as the result of the binding equilibrium.

We decided to focus our attention on the molecule acteoside (Fig. 6B), which is well known for its neuroprotective functions [44], and the interaction between α -syn and acteoside was further investigated by biophysical methods. Native-MS was employed to directly detect the protein-metabolite complex, thanks to the preservation of non-covalent interactions during the analysis. The nano-ESI-MS spectrum of α -syn under non-denaturing conditions (Supplementary Fig. S7A) showed a multimodal charge state distribution, in agreement with the heterogeneous conformational ensemble populated by the intrinsically disordered polypeptide chain. The titration of α -syn with acteoside highlighted the comparison of new peaks in the spectrum, with a position that corresponds to the mass of the 1:1 protein-ligand complex (Fig. 6C). These new signals increased in intensity at high metabolite concentrations, and mainly involve the low- and medium-charge states of the protein, corresponding to the compact and intermediate conformational components (Fig. 6D). The complex identity of the signals was further confirmed by collision-induced dissociation in gas-phase, with the detection of the unbound partners upon collision with helium atoms (Supplementary Fig. S7B). Despite the semi-quantitative nature of Native-MS experiments, the simultaneous

detection of free and bound protein states allowed the determination of a binding curve (Fig. 6E) and a rough estimation of the (apparent) dissociation constant of the complex ($K_d \sim 0.9$ mM). These results indicate a low affinity of α -syn for the metabolite, and are in agreement with the ones obtained by SPR. Indeed, this analysis also showed a direct binding of acteoside to α -syn, with a progressive increase of SPR-signal with ligand concentration. However, the accurate determination of the binding parameters was not possible, due to the lack of saturation caused by the very low affinity of the metabolite for the protein (Supplementary Fig. S8).

To conclude, considering its interaction with α -syn protein, the molecule acteoside from *V. thapsus* was considered for extended investigation.

Acteoside inhibits α -syn aggregation

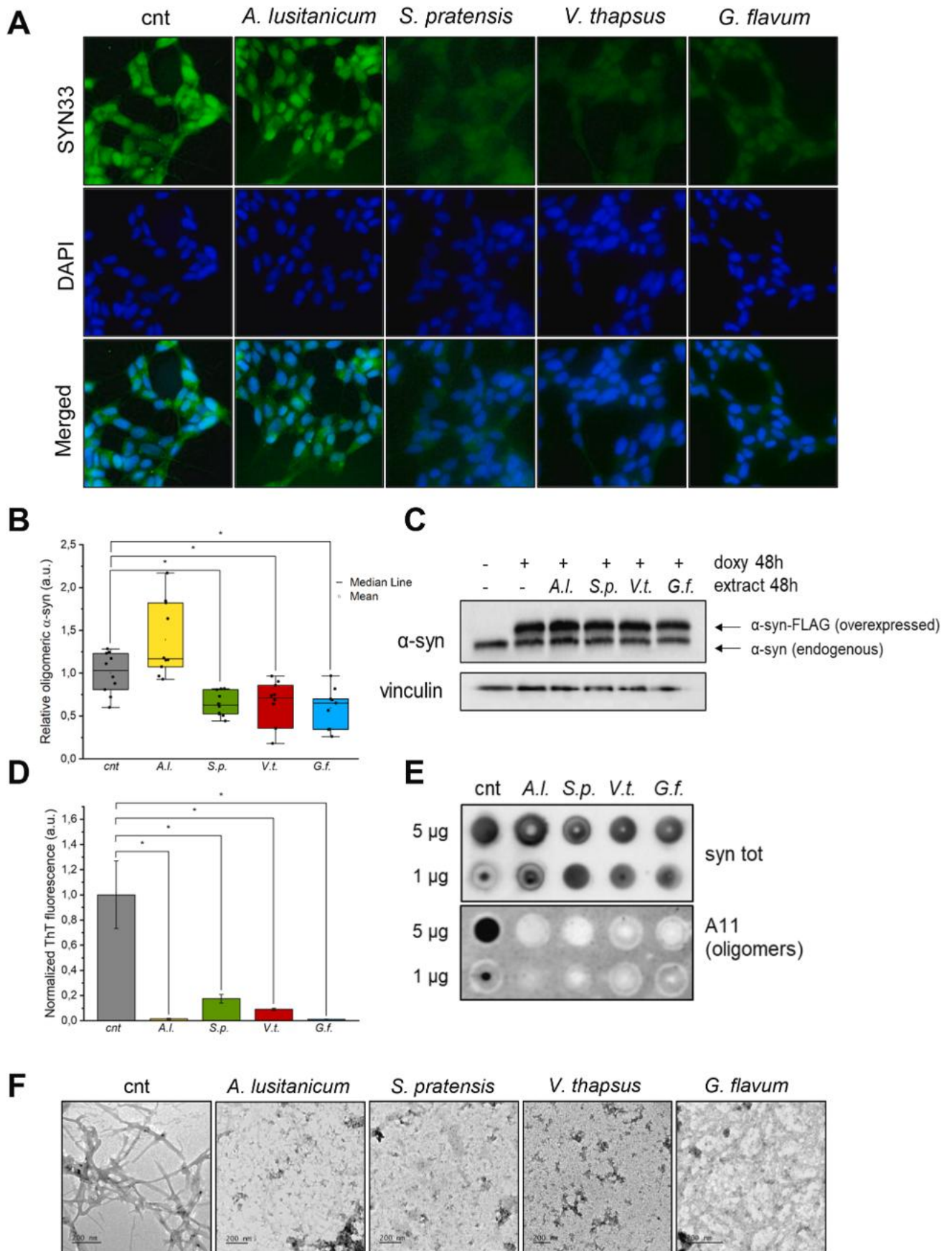
Building upon the identification of acteoside as a key metabolite binding to α -syn, we further elucidated its potential neuroprotective properties. Acteoside (Fig. 6B), the predominant phenylpropanoid glycoside in *V. thapsus* extract (Fig. 3C, Table 2), is commonly found in a variety of plants, especially of the *Verbascum* species, but also in more than 200 other plant species belonging to 23 different families, and it is well known for its strong antioxidant activity [45]. In order to investigate the direct effect of acteoside on the protein aggregation process, the Thioflavin T (ThT) assay was used. The incubation of α -syn (35 μ M) in the presence of 100 μ M or 50 μ M acteoside revealed that the molecule was exceptionally active, abrogating almost completely the formation of fibrils, with residual ThT fluorescence level of less than 1 % at both concentrations tested, similarly to the effect exerted by the whole *V. thapsus* extract (Fig. 7A). To better understand the inhibition of α -syn aggregation, we also investigated the protein aggregation kinetics. Notably, we did not observe the characteristic curve of α -syn aggregation when the protein was incubated with 100 μ M and 50 μ M of acteoside (Fig. 7B). This finding suggests that acteoside inhibits the formation of nucleation sites, which are essential for the initiation of the fibrillation phase and occur approximately 24 h from the beginning of the aggregation assay, as seen in the control sample (Fig. 7B). Remarkably, the inhibition of α -syn primary nucleation was also confirmed by the visualization of α -syn fibrils by TEM. Indeed, fibril formation was clearly visible when α -syn was incubated alone, while the presence of acteoside completely abolished the formation of the fibrillar species (Fig. 7C).

We next analyzed whether acteoside can influence fibril elongation [46], by studying aggregation of monomeric α -syn in the presence of preformed fibrils (PFF) of α -syn that act as seeds for secondary nucleation. Strikingly, we observed that acteoside inhibited fibril elongation in a dose-dependent manner: 1 μ M acteoside did not affect the fibril elongation phase, whereas at higher concentrations (25 μ M, 50 μ M and 100 μ M) fibril elongation was completely abolished, as highlighted by the absence of the characteristic curve of aggregation (Fig. 7D).

Altogether, these data indicate that acteoside plays a key role in the anti-aggregant effects of *V. thapsus* extract, influencing both primary nucleation and fibril elongation phases.

Acteoside activates the NRF2 signaling pathway

Before investigating acteoside effects on cell cultures, its cellular availability was assessed in human neuroblastoma cells by measuring intracellular/cell-associated level of acteoside in cells treated with 100 μ M of acteoside, a concentration which was not toxic up to 72 h (Supplementary Fig. S4B). As shown in Fig. 8A, the highest intracellular/cell-associated acteoside levels were observed after 1 h of treatment, and it gradually decreased over time. Then, in order to confirm the protective role of acteoside against oxidative stress, which is strictly connected with the onset of PD [47], SH-SY5Y cells were exposed to 5 μ M extracellular α -syn aggregates, obtained in the absence or



(caption on next page)

presence of 1 mM acteoside. Intracellular ROS level induced by PFF decreased by 54 % with acteoside in comparison with the control (Fig. 8B).

Strikingly, in SH-SY5Y neuroblastoma cells conditionally expressing α -syn, treatment with 100 μ M acteoside reduced the level of aggregated α -syn, as measured by immunofluorescence analysis using an antibody specific for the oligomers (Fig. 8C), without affecting the total level of α -syn, both endogenous and overexpressed (which bears a FLAG tag that enables to discriminate it from the endogenous protein, Fig. 8D).

To investigate the molecular mechanism underlying acteoside's antioxidant activity, we focused on NRF2, a well known pathway responsible for mediating antioxidant responses and maintaining redox homeostasis [48]. Indeed, we observed an increase in NRF2 protein level in cells treated with acteoside (Fig. 8E and F). Moreover, a clear nuclear enrichment of NRF2 was observed upon acteoside treatment (Fig. 8G and H). Accordingly, the mRNA level of two NRF2-dependent genes (NQO1 and HMOX1) increased in cells treated with acteoside (Fig. 8I), supporting NRF2 functional activation. In addition, pretreatment with acteoside prevented the increase of ROS level in cells treated with fibrils, but this effect was not observed when acteoside was added together with the NRF2 inhibitor (Fig. 8J). Altogether, these findings suggest that acteoside reduces intracellular ROS level through the activation of the NRF2 signaling pathway in neuroblastoma cells, in line with its antioxidant and neuroprotective effect.

Acteoside improves locomotor performance and reduces oxidative protein damage in a *Drosophila melanogaster* model of PD

Considering the antioxidant efficacy of acteoside in various biological systems [49–52], including rotenone-treated flies (a *Drosophila* model of sporadic PD) [53], we tested acteoside in a *Drosophila* PD model based on *DJ-1* β inactivation. The DJ-1 protein plays a central role in cellular defense against oxidative stress and is involved in ROS scavenging, transcriptional regulation, redox-dependent chaperone activity, mitochondrial function, and anti-apoptotic signaling [54]. Accordingly, *DJ-1* β mutant flies exhibit several PD-relevant phenotypes, including locomotor deficits, reduced lifespan, ROS accumulation, and hypersensitivity to oxidative toxins [29,55,56]. Thanks to its high pharmacological responsiveness, this *Drosophila* PD model has been successfully used to evaluate the therapeutic potential of multiple compounds with different mechanisms of action [29,56–58]. Besides, it should be mentioned that mutations in the DJ-1 protein cause autosomal recessive forms of PD, and oxidatively damaged DJ-1 protein accumulates in the brains of patients with idiopathic PD [59]. Therefore, to assess the potential therapeutic effect of acteoside, *DJ-1* β mutant flies were cultured on medium supplemented with the compound throughout development, from larval stage to five days post-eclosion. To determine the optimal dose for acteoside supplementation in flies, two concentrations of the compound were used (250 μ M and 400 μ M) and locomotor performance was assessed via climbing assays in 5-day-old flies. Acteoside administration resulted in a significant, dose-dependent improvement in motor function, producing a beneficial effect at both tested concentrations (Fig. 9A).

DJ-1 β mutant flies also exhibit increased ROS production, resulting in oxidative damage of cellular components [57,60]. A notable marker

of oxidative damage is protein carbonylation, whose level is elevated in *DJ-1* β mutant flies [61]. To determine whether acteoside influences oxidative protein damage, we measured protein carbonylation level in extracts from 5-day-old *DJ-1* β mutant flies treated with vehicle or with the compound at the tested concentrations (250 μ M and 400 μ M). Consistent with the climbing assay results, flies treated with 400 μ M acteoside exhibited a significant reduction of protein carbonyl groups (Fig. 9B), indicating that this compound can attenuate oxidative stress-induced protein damage, likely contributing to the observed improvements in motor performance. Despite the strong effect on motor function, treatment with 400 μ M acteoside had no significant impact on fly longevity (Supplementary Fig. S9), suggesting that it may improve healthspan rather than extend lifespan.

To further evaluate whether acteoside could exert a beneficial effect also when administered in adulthood, more accurately reflecting the timing of PD, flies were treated with acteoside (at a concentration of 400 μ M) after eclosion and climbing assays were performed 5 and 10 days following treatment initiation. As shown in Fig. 9C, acteoside significantly improved motor ability at both time points, demonstrating that it retains its efficacy also when administered post-eclosion. In agreement with these results, protein carbonylation level was also significantly decreased after 10 days of treatment (Fig. 9D). Therefore, the beneficial effect of acteoside emerges not only with early supplementation but also when treatment is initiated at advanced stages, reflecting the temporal dynamics and progression of PD pathology.

In conclusion, the observed functional recovery in *DJ-1* β mutants suggests that acteoside can effectively counteract deficits linked to *DJ-1* β dysfunction, thereby modulating PD-related phenotypes and validating its therapeutic potential.

Discussion

Plant biodiversity is an exceptional source of secondary metabolites, nevertheless no more than 15 % of higher plants have been systematically investigated for medicinal properties [62]. Consequently, the approach of bioprospecting, which promotes the research in biodiversity for new resources with potential income, remains a valuable opportunity to identify new bioactive compounds, or new sources of known compounds, increasing the value of biodiversity and supporting its conservation. Natural substances play a central role in creating innovative solutions for disease prevention/treatment and the advancement of analytical techniques, combined with high-throughput screening methods, can significantly improve the process of drug discovery. The biodiversity of the Mediterranean hotspot [11] is an extraordinary resource of bioactive compounds for advancing innovative therapies targeting non-communicable diseases, including neurodegenerative disorders.

A growing number of patients worldwide suffer from PD and the currently available drugs, which regulate dopaminergic and cholinergic transmission, primarily aim to control symptoms and improve patients' quality of life. However, there is still no definitive cure for this disease, making it necessary to develop new drugs, with particular attention to preventive strategies.

In this paper, we present a multidisciplinary approach to examining 60 different Italian plants representative of part of the Mediterranean

Fig. 5. The extracts from *S. pratensis*, *V. thapsus* and *G. flavum* reduce α -syn aggregation. (A–B) SH-SY5Y *pTet-SNCA-FLAG* cells were treated with 6 μ g/mL doxycycline to induce α -syn overexpression, in the absence or presence of the extracts from *A. lusitanicum*, *S. pratensis*, *V. thapsus* and *G. flavum* for 48 h. Representative immunofluorescence images (63x) of fixed cells, immunostained with anti-Syn33 antibody (specific for oligomeric species). Nuclei were stained by DAPI (blue). Graphs in B represent mean \pm SD of oligomeric α -syn fluorescence quantified as Integrated Density (IntDen) using ImageJ software. (C) SH-SY5Y *pTet-SNCA-FLAG* cells were treated with 6 μ g/mL doxycycline to induce α -syn overexpression, in the absence or presence of the extracts from *A. lusitanicum*, *S. pratensis*, *G. flavum* and *V. thapsus* for 48 h. The level of α -syn (both endogenous and FLAG-tagged overexpressed proteins) was evaluated by Western blot. Vinculin was used as loading control. (D) α -syn aggregation process, followed by ThT fluorescence, in the absence (cnt) or presence of *A. lusitanicum*, *S. pratensis*, *V. thapsus* or *G. flavum* extracts for 72 h. (E) Dot-blot analysis of α -syn (1 and 5 μ g) after 72 h of aggregation in the absence (cnt) or presence of *A. lusitanicum*, *S. pratensis*, *V. thapsus* or *G. flavum* extracts using A11 anti-oligomer antibody and anti- α -syn antibody as a control. (F) TEM images of α -syn after 72 h of aggregation in the absence (cnt) or presence of *A. lusitanicum*, *S. pratensis*, *V. thapsus* or *G. flavum* extracts. Data represent mean \pm SD from three independent experiments.

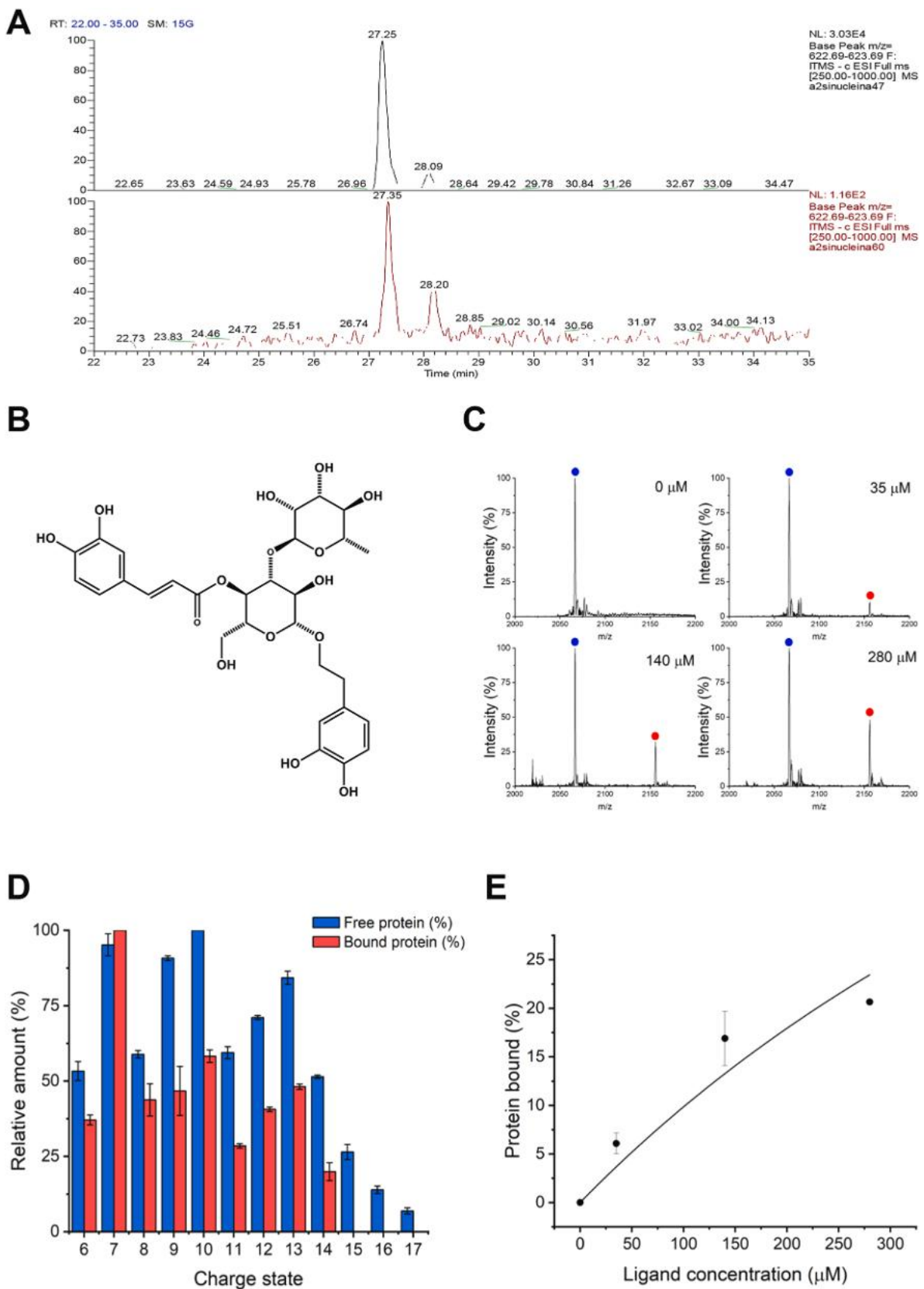


Fig. 6. Acteoside binds to α -syn. (A) RPLC-MS chromatograms in negative ion mode of *V. thapsus* crude extract (upper panel) and *V. thapsus* crude extract fished by α -syn (lower panel). Extracted ion acteoside, 623.19 *m/z*. (B) Chemical structure of acteoside. (C) Acteoside- α -syn interaction by Native-MS. Enlargement in the region of α -syn 7+ charge state of Native-MS spectra, obtained at distinct acteoside concentrations (0–280 μ M). The peaks corresponding to unbound α -syn (blue circle) and 1:1 α -syn-acteoside complex (red circle) are labeled. (D) Histogram reporting the fraction of unbound α -syn (blue) and α -syn-acteoside complex (red) as a function of the analyte charge state. (E) Fraction of protein in the bound state vs. total ligand concentration. The solid line represents the non-linear fit of the experimental data with a 1:1 binding curve ($K_d \sim 0.9$ mM).

flora. We combined an *in silico* screening system based on phylogenetic methods with a high-throughput screening using as a model the budding yeast expressing human α -syn.

This approach allowed a rapid and economic high-throughput analysis and led us to focus on phytoextracts from four plants, namely *A. lusitanicum*, *S. pratensis*, *V. thapsus* and *G. flavum*, which are promising sources of neuroprotective compounds for the preventive treatment of PD, being strongly active in reducing the toxic intracellular species of aggregated proteins. Notably, acteoside, one of the major metabolites found in the *V. thapsus* extract, emerges as the key molecule that binds α -syn. Of paramount importance, *V. thapsus* is already included in the Belfruit list [32], supporting its utilization as a public health product [33]. Acteoside, also known as verbascoside, was first isolated in 1963 from *Verbascum sinuatum* L., belonging to the family *Scrophulariaceae* [45]. Chemically, acteoside (Fig. 6B), with a formula of $C_{29}H_{36}O_{15}$ and a molecular weight of 624 Da, is a phenylethanoid glycoside [63]. Acteoside contains a hydroxyl salidroside residue condensed with caffeoyl and rhamnose moieties, and is among the most widespread disaccharide caffeoyl esters. While mainly detected in *Verbascum*

species, acteoside has also been found in 23 different plant families [45, 64]. It is extracted from various traditional Chinese medicine sources including *Rehmannia glutinosa*, *Cistanche deserticola* and *Pedicularis kansuensis* [65] and is considered a crucial secondary metabolite in folk medicine [66,67] with a variety of pharmacological activities [68–72]. Several studies have reported that acteoside exerts strong antioxidant activities, and it is especially able to enhance the endogenous antioxidant defences of the cell (for a review see Ref. [45]). The neuroprotective effects of acteoside have been linked not only to its ability to mitigate oxidative stress, but also to inhibit neuroinflammation and to modulate autophagy [53,67].

Here we also show that acteoside directly binds to α -syn and inhibits its amyloid fibrils formation (Figs. 6 and 7), a key event in the prevention of PD. Specifically, since α -syn aggregation involves both nucleation and growth phases [73], we show under different aggregation conditions that acteoside inhibits primary nucleation, by preventing nuclei formation during the lag phase (Fig. 7B and C), as well as fibril-induced amplification during the growth phase (Fig. 7D), indicating that acteoside functions as a protein aggregation inhibitor at multiple stages of the

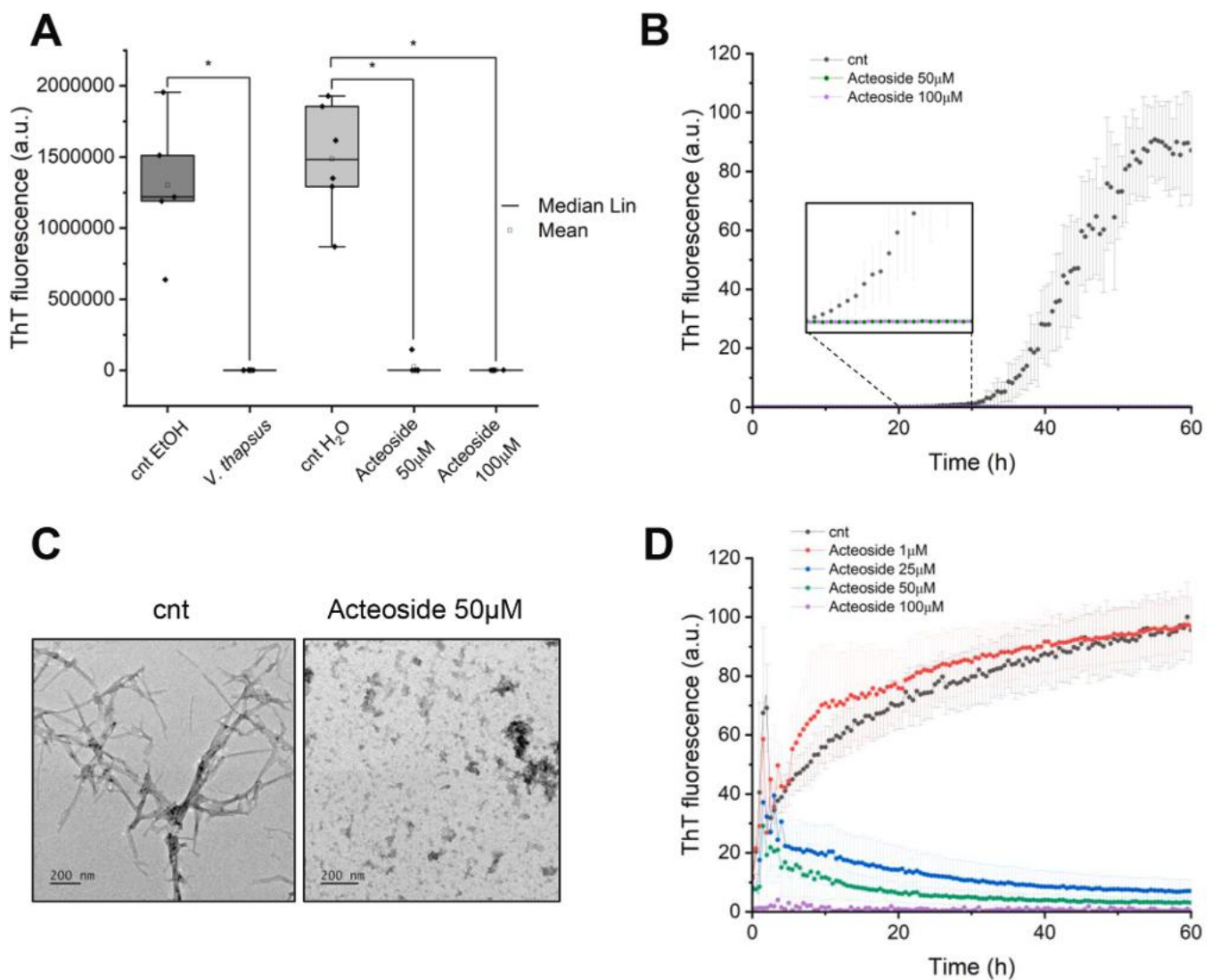
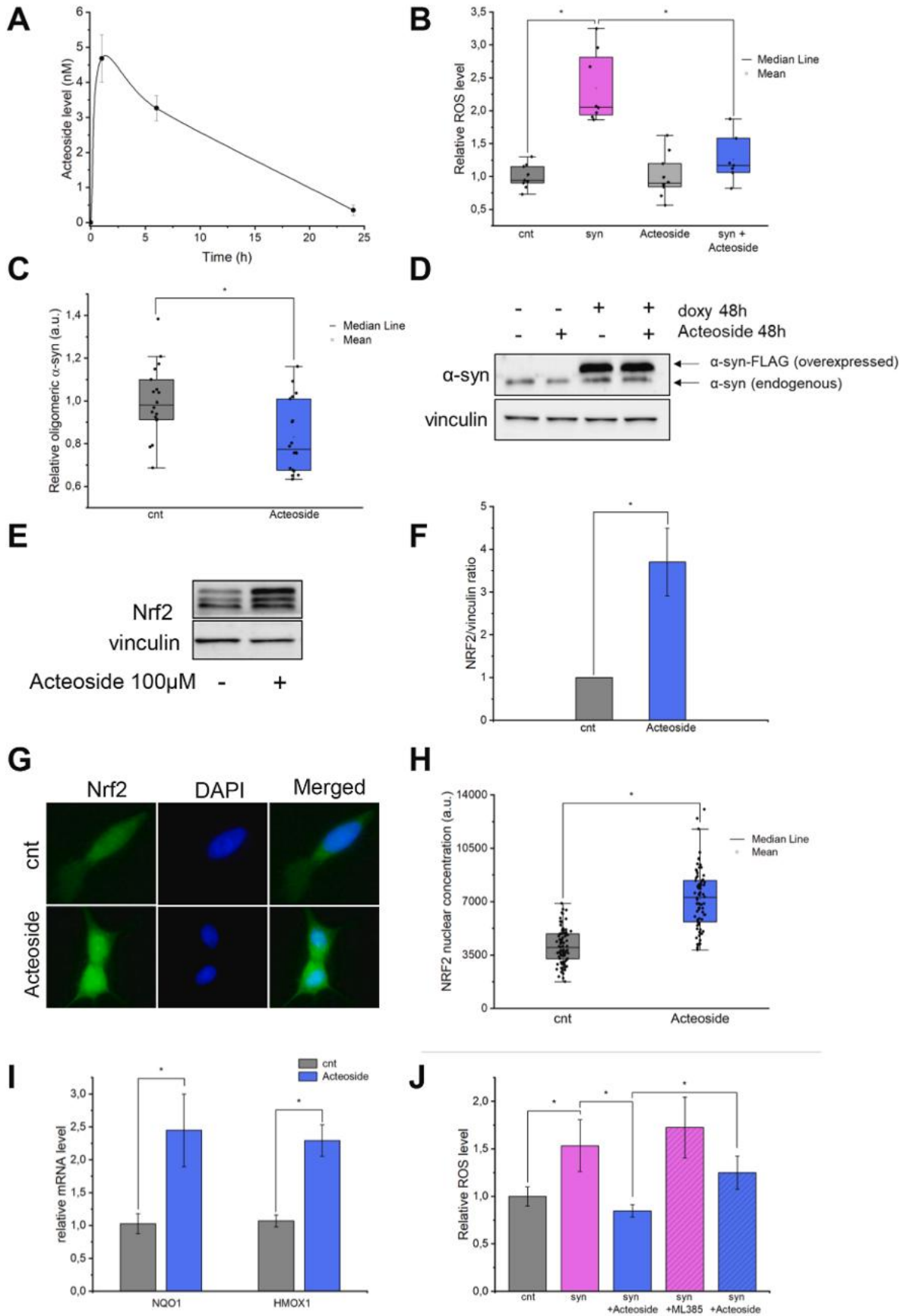


Fig. 7. Acteoside inhibits α -syn aggregation. (A) α -syn aggregation process, followed by ThT fluorescence after 72 h, in the absence (cnt 1, solvent control 2.5 % ethanol) or presence of *V. thapsus* (solvent 2.5 % ethanol) and in the absence (cnt 2, solvent control water) or presence of acteoside (100 μ M or 50 μ M in aqueous solution). (B) Kinetic of α -syn aggregation process, detected by ThT fluorescence, in the absence (cnt) or presence of acteoside (100 μ M or 50 μ M), with a zoom of the 20–30 h time interval. (C) TEM images of 70 μ M α -syn after 72 h of aggregation in the absence (cnt) or presence of acteoside (50 μ M in aqueous solution). (D) α -syn fibril elongation: 35 μ M monomeric protein was incubated with 1 μ M of preformed fibrils, detected by ThT fluorescence, in the absence (cnt) or presence of increasing concentration of acteoside (1 μ M, 25 μ M, 50 μ M and 100 μ M). Representative data from $n = 3$ independent experiments.



(caption on next page)

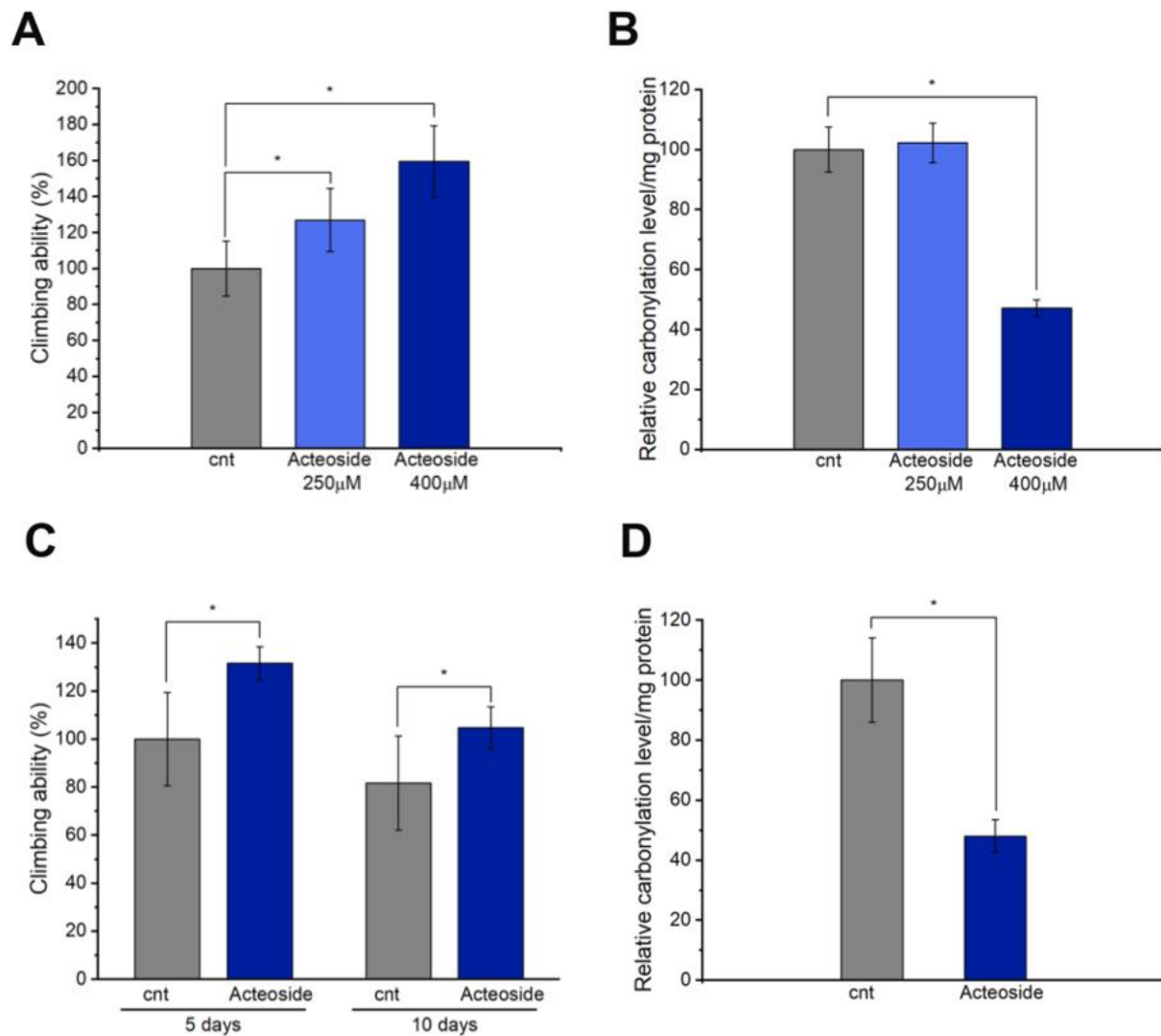


Fig. 9. Effect of acteoside on *DJ-1 β* mutant flies. (A) Motor performance of *DJ-1 β* mutant flies treated with 250 and 400 μ M acteoside was evaluated by performing a climbing assay ($n = 80$ – 120 5-day-old female flies for each condition). (B) Protein carbonylation level in *DJ-1 β* mutant flies treated with 250 and 400 μ M acteoside was analyzed using 2,4-dinitrophenylhydrazine (DNPH) derivatization, data are expressed as arbitrary units (a.u.) per mg of protein. Results were normalized to data obtained from flies cultured in vehicle medium (0.1 % DMSO). Values are expressed as mean \pm SD from three independent experiments in which three biological replicates were used. Groups were statistically compared by one-way ANOVA analysis followed by Tukey's post hoc test ($*p < 0.05$). (C) Motor performance of *DJ-1 β* mutant flies treated post-eclosion with 400 μ M acteoside was evaluated by performing a climbing assay 5 and 10 days after treatment initiation ($n = 80$ – 120 female flies per condition). (D) Protein carbonylation level in *DJ-1 β* mutant flies treated post-eclosion with 400 μ M acteoside was analyzed 10 days after treatment using 2,4-dinitrophenylhydrazine (DNPH) derivatization, data are expressed as arbitrary units (a.u.) per mg of protein. Results were normalized to data obtained from control flies cultured in vehicle medium (0.1 % DMSO). Values are expressed as mean \pm SD from three independent experiments. $*p < 0.05$.

process. Intriguingly, previous studies have shown that acteoside reduces the aggregation of another prion-like protein, the amyloid β ($A\beta$) peptide, thereby decreasing its toxicity in Alzheimer's disease models [74–76].

The discovery that acteoside also inhibits α -synuclein fibrillation paves the way for its potential development as a preventive treatment for PD. Given that PD is a disorder with complex evolution, a broad-

Fig. 8. Acteoside activates the NRF2 signaling pathway. (A) Temporal course of intracellular/cell-associated level of acteoside in neuroblastoma cells. Data are expressed as pmol acteoside/ μ g proteins. (B) SH-SY5Y cells were grown for 72 h in the absence or presence of 5 μ M α -syn, obtained after 72 h of aggregation without or with 1 mM acteoside. ROS level was evaluated by H_2DCFDA staining. $*p < 0.05$. (C) SH-SY5Y *pTet-SNCA-FLAG* cells were treated with 6 μ g/mL doxycycline to induce α -syn overexpression, in the absence or presence of 100 μ M acteoside for 48 h. Cells were fixed and immunostained with anti-Syn33 antibody (specific for oligomeric species). Graphs represent mean \pm SD of oligomeric α -syn fluorescence quantified as Integrated Density (IntDen) using ImageJ software. (D) SH-SY5Y *pTet-SNCA-FLAG* cells were treated with 6 μ g/mL doxycycline to induce α -syn overexpression, in the absence or presence of 100 μ M acteoside for 48 h. The level of α -syn (both endogenous and FLAG-tagged overexpressed) was evaluated by Western blot. Vinculin was used as loading control. (E) Western analysis using anti-NRF2 and anti-vinculin antibody on protein extracts from neuroblastoma cells grown for 48 h in the absence (cnt) or in the presence of acteoside (100 μ M). (F) Quantitative analysis of NRF2 protein level in (E). (G) Immunofluorescence images of neuroblastoma cells treated with 100 μ M of acteoside for 48 h. Fixed cells were immunostained with anti-NRF2 antibody. Nuclei were stained by DAPI (blue). (H) Quantitative analysis of nuclear localization in (G) performed using Cell-ACDC software. (I) Relative mRNA expression levels of NQO1 and HMOX1 genes in neuroblastoma cells grown in the absence (cnt) or in the presence of acteoside (100 μ M) for 48 h. (J) SH-SY5Y cells were pretreated with 100 μ M acteoside and/or 5 μ M ML385 (NRF2 inhibitor) for 2 h, then treated with 5 μ M α -syn fibrils for 72 h. ROS level was evaluated by H_2DCFDA staining. Data represent mean \pm SD from $n = 3$ independent experiments, $*p < 0.05$.

spectrum approach to target different pathological pathways could be a promising strategy. In this context, oxidative stress is strongly associated with this disease and it is linked with various cellular processes, which all seem to contribute to neurodegeneration [77]. Notably, in SH-SY5Y cells exposed to toxic α -syn aggregates, acteoside decreases intracellular ROS level (Fig. 8B). This is associated with the activation of the NRF2 signaling pathway, leading to the stimulation of the antioxidant response (Fig. 8). In agreement with our data, previous reports have highlighted the role of acteoside in modulating the NRF2 pathway *in vitro* and both in mouse and Zebrafish PD models [78,79]. Moreover, docking analyses have also reported possible binding of acteoside to NRF2 protein [80]. Remarkably, acteoside treatment restored locomotor function and reduced protein carbonylation *in vivo* in a *Drosophila* model of PD based on loss of *DJ-1 β* function (Fig. 9). This dual action in a different PD model affecting a gene involved in both familial and sporadic form of the disease underscores its potential as a multifunctional therapeutic candidate for PD. Although preliminary, these results, obtained in a multicellular model organism, provide a solid basis for future studies aimed at dissecting the molecular pathways targeted by acteoside and evaluating its translational relevance in mammalian PD models.

Understanding acteoside's pharmacokinetic properties is crucial to assess its therapeutic potential and translational value. Despite its well documented antioxidant and neuroprotective activities, and its high level of safety [71,81–83], acteoside exhibits poor bioavailability [51]. *In vivo* studies in rats and beagle dogs have shown low systemic availability after oral administration, with bioavailability ranging from 0.1 % to 4 %. This poor bioavailability is primarily attributed to acteoside's high hydrophilicity, low membrane permeability and active efflux transport through P-glycoprotein (P-gp) [44]. Our findings are consistent with the previous observations. Intracellular or cell-associated acteoside reaches approximately 0.1 % after 1 h of treatment (Fig. 8A). This low but measurable uptake confirms acteoside's ability to enter cells or interact with their membranes, supporting its bioactivity. In addition, promising studies in rat models indicate that acteoside is able to reach the brain [84] and its blood-brain barrier permeability can be further enhanced through lipid encapsulation [85], suggesting that proper formulations of this compound are essential to maximize its activity *in vivo*. In conclusion, this study provides new evidence that acteoside possesses an inhibitory effect on α -syn aggregation and supports its antioxidant role, suggesting the relevance of this molecule as a candidate for neuroprotection in PD. Future studies will be essential to investigate the molecular pathways involved in the anti-aggregant properties of acteoside and to develop new strategies to increase its potential value as a preventive agent against synucleinopathies *in vivo*.

Author contributions

Alessia Lambiase: Investigation; Validation; Visualization; Writing – original draft; Writing – review & editing.

Giorgia Spandri: Investigation; Visualization; Writing – review & editing.

Hind Moukham: Investigation; Visualization.

Elisa Toini: Investigation; Methodology; Visualization.

Annalisa D'Urzo: Investigation; Methodology.

Giovanni Zecca: Investigation; Methodology; Writing – original draft; Writing – review & editing.

Mauro Commisso: Investigation.

Flavia Guzzo: Conceptualization; Funding acquisition.

Valentina Santoro: Investigation; Methodology.

Anna Lisa Piccinelli: Writing – review & editing; Conceptualization.

Enrica Calleri: Writing – review & editing.

Sofia Salerno: Investigation.

Francesca Rinaldi: Investigation.

Stefano Negri: Investigation.

Carlo Santambrogio: Investigation; Visualization; Writing – review & editing.

Maura Briosci: Investigation.

Cristina Solana-Manrique: Validation, Methodology.

Massimo Labra: Conceptualization; Project administration; Funding acquisition.

Fabrizio Grassi: Conceptualization; Writing – original draft; Writing – review & editing.

Nuria Paricio: Writing – review & editing.

Farida Tripodi: Investigation; Validation; Visualization; Writing – original draft; Writing – review & editing.

Paola Coccetti: Writing – original draft; Writing – review & editing; Conceptualization; Project administration; Funding acquisition.

Ethical statement

Not required as no humans or animals are involved in this work.

Data availability

Data will be made available on request.

Declaration of competing interests

The authors declare that they have no known competing financial interests or personal relationships that could have appeared to influence the work reported in this paper.

Acknowledgments

Project funded under the National Recovery and Resilience Plan (NRRP), Mission 4. Component 2 Investment 1.4—Call for tender No. 3138 of December 16, 2021, rectified by Decree n.3175 of December 18, 2021 of Italian Ministry of University and Research funded by the European Union—NextGenerationEU; Award Number: Project code CN_00000033, Concession Decree No. 1034 of June 17, 2022. Adopted by the Italian Ministry of University and Research, CUP, H43C22000530001, Spoke 6, Project title “National Biodiversity Future Center—NBFC”. Project funded under the National Recovery and Resilience Plan (NRRP), Mission 4. Component 2 Investment 1.3—Call for tender No. 3138, 16 December 2021, rectified by Decree n.341 of 15 March 2022 of Italian Ministry of University and Research funded by the European Union—NextGenerationEU; Project code PE0000003 ON FOODS—CUP: H43C22000820001—Spoke 6, Project title “ON Foods—Research and innovation network on food and nutrition Sustainability, Safety and Security—Working ON Foods”. Project funded by the University of Valencia to Nuria Paricio, Grantcode UV-INV-AE-3664989.

Appendix A. Supplementary data

Supplementary data to this article can be found online at <https://doi.org/10.1016/j.neurot.2025.e00825>.

Abbreviations

α -syn	α -synuclein
CLS	Chronological lifespan assay
MP	Medicinal Plants
PD	Parkinson's disease
PFF	preformed fibrils
PMP	Potential Medicinal Plants
ROS	reactive oxygen species
RPLC-MS	reverse phase liquid chromatography mass spectrometry
SEC AS-MS	size exclusion chromatography coupled to reversed phase LC-MS
SPR	Surface Plasmon Resonance
TEM	Transmission electron microscopy
ThT	Thioflavin T

References

- [1] Calabresi P, Mechelli A, Natale G, Volpicelli-Daley L, Di Lazzaro G, Ghiglieri V. Alpha-synuclein in Parkinson's disease and other synucleinopathies: from overt neurodegeneration back to early synaptic dysfunction. *Cell Death Dis* 2023;14:176.
- [2] Fields CR, Bengoa-Vergniory N, Wade-Martins R. Targeting alpha-synuclein as a therapy for Parkinson's disease. *Front Mol Neurosci* 2019;12:299.
- [3] Poewe W, Seppi K, Tanner CM, Halliday GM, Brundin P, Volkman J, et al. Parkinson disease. *Nat Rev Dis Primers* 2017;3:17013.
- [4] Ghiglieri V, Calabrese V, Calabresi P. Alpha-synuclein: from early synaptic dysfunction to neurodegeneration. *Front Neurol* 2018;9:295.
- [5] Moise G, Jijie A-R, Moacă E-A, Predescu I-A, Dehelean CA, Hegheş A, et al. Plants' impact on the human brain - exploring the neuroprotective and neurotoxic potential of plants. *Pharmaceuticals* 2024;17:1339.
- [6] Moukham H, Lambiase A, Barone GD, Tripodi F, Coccetti P. Exploiting natural niches with neuroprotective properties: a comprehensive review. *Nutrients* 2024;16:1298.
- [7] Najmi A, Javed SA, Al Bratty M, Alhazmi HA. Modern approaches in the discovery and development of plant-based natural products and their analogues as potential therapeutic agents. *Molecules* 2022;27:349.
- [8] Ronsted N, Symonds MRE, Birkholm T, Christensen SB, Meerow AW, Molander M, et al. Can phylogeny predict chemical diversity and potential medicinal activity of plants? A case study of amaryllidaceae. *BMC Evol Biol* 2012;12:182.
- [9] Zaman W, Ye J, Saqib S, Liu Y, Shan Z, Hao D, et al. Predicting potential medicinal plants with phylogenetic topology: inspiration from the research of traditional Chinese medicine. *J Ethnopharmacol* 2021;281:114515.
- [10] Ernst M, Saslis-Lagoudakis CH, Grace OM, Nilsson N, Simonsen HT, Horn JW, et al. Evolutionary prediction of medicinal properties in the genus *Euphorbia* L. *Sci Rep* 2016;6:30531.
- [11] Cena H, Labra M. Biodiversity and planetary health: a call for integrated action. *Lancet* 2024;403:1985–6.
- [12] Heywood V. The future of floristics in the Mediterranean region. *Isr J Plant Sci* 2002;50(suppl 1):5–13.
- [13] Muñoz-Soriano V, Paricio N. *Drosophila* models of Parkinson's disease: discovering relevant pathways and novel therapeutic strategies. *Park Dis* 2011;5:20640.
- [14] Bonifati V, Rizzi P, van Baren MJ, Schaap O, Breedveld GJ, Krieger E, et al. Mutations in the DJ-1 gene associated with autosomal recessive early-onset Parkinsonism. *Science* 2003;299:256–9.
- [15] De Soricellis G, Rinaldi F, Tengattini S, Temporini C, Negri S, Capelli D, et al. Development of an analytical platform for the affinity screening of natural extracts by SEC-MS towards PPAR α and PPAR γ receptors. *Anal Chim Acta* 2024;1309:342666.
- [16] Giammona A, Commisso M, Bonanomi M, Remedia S, Avesani L, Porro D, et al. A novel strategy for glioblastoma treatment by natural bioactive molecules showed a highly effective anti-cancer potential. *Nutrients* 2024;16:2389.
- [17] U.S. Department of Agriculture, Agricultural research service. Dr. Duke's phytochemical ethnobotanical databases. In: USDA agricultural research service [online]. Available at: <http://phytochem.nal.usda.gov/>. Accessed February 19, 2025.
- [18] Duke JA. Dr. Duke's phytochemical and ethnobotanical databases. In: Ag data commons [online]. Available at: <https://doi.org/10.15482/USDA.ADC/1239279>. Accessed February 19, 2025.
- [19] Zanne AE, Tank DC, Cornwell WK, Eastman JM, Smith SA, FitzJohn RG, et al. Three keys to the radiation of angiosperms into freezing environments. *Nature* 2014;506:89–92.
- [20] Webb CO, Ackerly DD, Kembel SW. Phylocom: software for the analysis of phylogenetic community structure and trait evolution. *Bioinforma Oxf Engl* 2008;24:2098–100.
- [21] Pellicer J, Saslis-Lagoudakis CH, Carrió E, Ernst M, Garnatje T, Grace OM, et al. A phylogenetic road map to antimalarial *Artemisia* species. *J Ethnopharmacol* 2018;225:1–9.
- [22] Saslis-Lagoudakis CH, Klitgaard BB, Forest F, Francis L, Savolainen V, Williamson EM, et al. The use of phylogeny to interpret cross-cultural patterns in plant use and guide medicinal plant discovery: an example from *Pterocarpus* (Leguminosae). *PLoS One* 2011;6:e22275.
- [23] Tripodi F, Lambiase A, Moukham H, Spandri G, Briosci M, Falletta E, et al. Targeting protein aggregation using a cocoa-bean shell extract to reduce α -synuclein toxicity in models of Parkinson's disease. *Curr Res Food Sci* 2024;9:100888.
- [24] Tripodi F, Falletta E, Leri M, Angeloni C, Beghelli D, Giusti L, et al. Anti-aging and neuroprotective properties of *Grifola frondosa* and *Hericium erinaceus* extracts. *Nutrients* 2022;14:4368.
- [25] LeVine H. Thioflavine T interaction with synthetic Alzheimer's disease beta-amyloid peptides: detection of amyloid aggregation in solution. *Protein Sci Publ Protein Soc* 1993;2:404–10.
- [26] Padovani F, Mairhormann B, Falter-Braun P, Lengefeld J, Schmoller KM. Segmentation, tracking and cell cycle analysis of live-cell imaging data with Cell-ADC. *BMC Biol* 2022;20:174.
- [27] Park J, Kim SY, Cha G-H, Lee SB, Kim S, Chung J. *Drosophila* DJ-1 mutants show oxidative stress-sensitive locomotive dysfunction. *Gene* 2005;361:133–9.
- [28] Solana-Manrique C, Moltó MD, Calap-Quintana P, Sanz FJ, Llorens JV, Paricio N. *Drosophila* as a model system for the identification of pharmacological therapies in neurodegenerative diseases. In: Mutsuddi M, Mukherjee A, editors. *Insights hum. Neurodegener. Lessons learnt drosoph.* Singapore: Springer; 2019. p. 433–67.
- [29] Sanz FJ, Solana-Manrique C, Muñoz-Soriano V, Calap-Quintana P, Moltó MD, Paricio N. Identification of potential therapeutic compounds for Parkinson's disease using *Drosophila* and human cell models. *Free Radic Biol Med* 2017;108:683–91.
- [30] Solana-Manrique C, Sanz FJ, Ripollés E, Bañó MC, Torres J, Muñoz-Soriano V, et al. Enhanced activity of glycolytic enzymes in *Drosophila* and human cell models of Parkinson's disease based on DJ-1 deficiency. *Free Radic Biol Med* 2020;158:137–48.
- [31] Ono E, Murata J. Exploring the evolvability of plant specialized metabolism: uniqueness out of uniformity and uniqueness behind uniformity. *Plant Cell Physiol* 2023;64:1449–65.
- [32] Ministero della Salute. Decreto 10 agosto 2018 (18A06095). Disciplina dell'impiego negli integratori alimentari di sostanze e preparati vegetali. In: *Gazzetta Ufficiale Della Repubblica Italiana* [online]. Serie Generale n.224; 26 settembre 2018. Available at: <https://www.gazzettaufficiale.it/eli/id/2018/09/26/18A06095/sg>. Accessed February 19, 2025.
- [33] Biagi M, Pecorari R, Appendino G, Miraldi E, Magnano AR, Governa P, et al. Herbal products in Italy: the thin line between phytotherapy, nutrition and parpharmaceuticals; a normative overview of the fastest growing market in Europe. *Pharmaceuticals* 2016;9:65.
- [34] Tenreiro S, Rosado-Ramos R, Gerhardt E, Favretto F, Magalhães F, Popova B, et al. Yeast reveals similar molecular mechanisms underlying alpha- and beta-synuclein toxicity. *Hum Mol Genet* 2016;25:275–90.
- [35] Franssens V, Bynens T, Van den Brande J, Vandermeeren K, Verduyck M, Winderickx J. The benefits of humanized yeast models to study Parkinson's disease. *Oxid Med Cell Longev* 2013;2013:760629.
- [36] Fabrizio P, Longo VD. The chronological life span of *Saccharomyces cerevisiae*. In: *Tollefsbol TO, editor. Biol. Aging methods protoc.* Totowa, NJ: Humana Press; 2007. p. 89–95.
- [37] Won SJ, Fong R, Butler N, Sanchez J, Zhang Y, Wong C, et al. Neuronal oxidative stress promotes α -synuclein aggregation *in vivo*. *Antioxidants* 2022;11:2466.
- [38] Suryanti V, Wibowo FR, Khotijah S, Andalucki N. Antioxidant activities of cinnamaldehyde derivatives. *IOP Conf Ser Mater Sci Eng* 2018;333:012077.
- [39] Siwecka N, Saramowicz K, Galita G, Rozpdek-Kamińska W, Majsterek L. Inhibition of protein aggregation and endoplasmic reticulum stress as a targeted therapy for α -synucleinopathy. *Pharmaceutics* 2023;15:2051.
- [40] Fu L, Sztl E. Characterization of intracellular aggregates by fluorescent microscopy. *Methods Mol Biol Clifton NJ* 2015;1258:307–17.
- [41] Vasquez V, Mitra J, Perry G, Rao KS, Hegde ML. An inducible alpha-synuclein expressing neuronal cell line model for Parkinson's disease. *J Alzheimers Dis JAD* 2018;66:453–60.
- [42] Biancalana M, Koide S. Molecular mechanism of Thioflavin-T binding to amyloid fibrils. *Biochim Biophys Acta BBA - Prot Proteom* 2010;1804:1405–12.
- [43] Geng P, Chen P, Lin L-Z, Sun J, Harrington P, Harnly J. Classification of structural characteristics facilitate identifying steroidal saponins in *Alliums* using ultra-high performance liquid chromatography high-resolution mass spectrometry. *J Food Compos Anal* 2021;102:103994.
- [44] Xiao Y, Ren Q, Wu L. The pharmacokinetic property and pharmacological activity of acteoside: a review. *Biomed Pharmacother* 2022;153:113296.
- [45] Alipieva K, Korkina L, Orhan IE, Georgiev MI. Verbascoide - a review of its occurrence, (bio)synthesis and pharmacological significance. *Biotechnol Adv* 2014;32:1065–76.
- [46] Perni M, Flagmaier P, Limbocker R, Cascella R, Aprile FA, Galvagnion C, et al. Multistep inhibition of α -synuclein aggregation and toxicity *in vitro* and *in vivo* by trodusquemine. *ACS Chem Biol* 2018;13:2308–19.
- [47] Khan MS, Nasiripour S, Bopassa JC. Parkinson disease signaling pathways, molecular mechanisms, and potential therapeutic strategies: a comprehensive review. *Int J Mol Sci* 2025;26:6416.
- [48] Papaiahgari S, Zhang Q, Kleeberger SR, Cho H-Y, Reddy SP. Hypoxia stimulates an Nrf2-ARE transcriptional response via ROS-EGFR-P13K-Akt/ERK MAP kinase signaling in pulmonary epithelial cells. *Antioxidants Redox Signal* 2006;8:43–52.
- [49] Muhtar E, Ylham G, Tiemuer A, Ediris S. Unraveling the dual anti-inflammatory and antioxidant mechanisms of acteoside: computational insights and experimental validation. *Chem Biodivers* 2025;22:e202401564.
- [50] Marčetić M, Bufan B, Drobac M, Antić Stanković J, Arsenović Ranin N, Milenković MT, et al. Multifaceted biological properties of verbascoide/acteoside: antimicrobial, cytotoxic, anti-inflammatory, and immunomodulatory effects. *Antibiotics* 2025;14:697.
- [51] Mohammed RA, Kamel AS, Hindam MO, El-Dessouki AM, Hamouda HA, Ramadan NM, et al. Acteoside as a multifunctional natural glycoside: therapeutic potential across various diseases. *Inflammopharmacology* 2025.
- [52] Saha R, Majie A, Baidya R, Sarkar B. Verbascoide: comprehensive review of a phenylethanoid macromolecule and its journey from nature to bench. *Inflammopharmacology* 2024;32:2729–51.
- [53] Aimaiti M, Wumaier A, Aisa Y, Zhang Y, Xirepu X, Aibaidula Y, et al. Acteoside exerts neuroprotection effects in the model of Parkinson's disease via inducing autophagy: network pharmacology and experimental study. *Eur J Pharmacol* 2021;903:174136.
- [54] Sun ME, Zheng Q. The tale of DJ-1 (PARK7): a swiss army knife in biomedical and psychological research. *Int J Mol Sci* 2023;24:7409.
- [55] Lavara-Culebras E, Paricio N. *Drosophila* DJ-1 mutants are sensitive to oxidative stress and show reduced lifespan and motor deficits. *Gene* 2007;400:158–65.
- [56] Sanz FJ, Solana-Manrique C, Paricio N. Disease-modifying effects of vincamine supplementation in *Drosophila* and human cell models of Parkinson's disease based on DJ-1 deficiency. *ACS Chem Neurosci* 2023;14:2294–301.
- [57] Casani S, Gómez-Pastor R, Matallana E, Paricio N. Antioxidant compound supplementation prevents oxidative damage in a *Drosophila* model of Parkinson's disease. *Free Radic Biol Med* 2013;61:151–60.

- [58] Sanz FJ, Solana-Manrique C, Torres J, Masiá E, Vicent MJ, Paricio N. A High-throughput chemical screen in DJ-1 β mutant flies identifies zaprinast as a potential Parkinson's disease treatment. *Neurotherapeutics* 2021;18:2565–78.
- [59] Skou LD, Johansen SK, Okarmus J, Meyer M. Pathogenesis of DJ-1/PARK7-mediated Parkinson's disease. *Cells* 2024;13:296.
- [60] Lavara-Culebras E, Muñoz-Soriano V, Gómez-Pastor R, Matallana E, Paricio N. Effects of pharmacological agents on the lifespan phenotype of *Drosophila DJ-1 β* mutants. *Gene* 2010;462:26–33.
- [61] Solana-Manrique C, Muñoz-Soriano V, Sanz FJ, Paricio N. Oxidative modification impairs SERCA activity in *Drosophila* and human cell models of Parkinson's disease. *Biochim Biophys Acta BBA - Mol Basis Dis* 2021;1867:166152.
- [62] Skirycz A, Kierszniowska S, Méret M, Willmitzer L, Tzotzos G. Medicinal bioprospecting of the Amazon rainforest: a modern Eldorado? *Trends Biotechnol* 2016;34:781–90.
- [63] Dembitsky VM. Astonishing diversity of natural surfactants: 5. Biologically active glycosides of aromatic metabolites. *Lipids* 2005;40:869–900.
- [64] Yang Y, Xi D, Wu Y, Liu T. Complete biosynthesis of the phenylethanoid glycoside verbascoside. *Plant Commun* 2023;4:100592.
- [65] Gao L-L, Jia D, Shi J-Q, Zhang J-C, Lu L-X, Wei M, et al. Acteoside suppresses hepatocellular carcinoma progression via modulation of macrophage migration inhibitory factor and mitogen-activated protein kinase proteins. *Int J Biol Macromol* 2025;320:145579.
- [66] Huang J, Zhao D, Cui C, Hao J, Zhang Z, Guo L. Research progress and trends of phenylethanoid glycoside delivery systems. *Foods* 2022;11:769.
- [67] Zhao Y, Wang S, Pan J, Ma K. Verbascoside: a neuroprotective phenylethanoid glycosides with anti-depressive properties. *Phytomedicine* 2023;120:155027.
- [68] Song HS, Choi MY, Ko MS, Jeong JM, Kim YH, Jang BH, et al. Competitive inhibition of cytosolic Ca²⁺-dependent phospholipase A2 by acteoside in RBL-2H3 cells. *Arch Pharm Res (Seoul)* 2012;35:905–10.
- [69] Lau C-W, Chen Z-Y, Wong C-M, Yao X, He Z, Xu H, et al. Attenuated endothelium-mediated relaxation by acteoside in rat aorta: role of endothelial [Ca²⁺] and nitric oxide/cyclic GMP pathway. *Life Sci* 2004;75:1149–57.
- [70] Lu Y, Zhou W, Feng Y, Li Y, Liu K, Liu L, et al. Acteoside and acyl-migrated acteoside, compounds in Chinese kudingcha tea, inhibit α -amylase *in vitro*. *J Med Food* 2017;20:577–85.
- [71] Khullar M, Sharma A, Wani A, Sharma N, Sharma N, Chandan BK, et al. Acteoside ameliorates inflammatory responses through NF κ B pathway in alcohol induced hepatic damage. *Int Immunopharmacol* 2019;69:109–17.
- [72] Avila JG, de Liverant JG, Martínez A, Martínez G, Muñoz JL, Arciniegas A, et al. Mode of action of *Buddleja cordata* verbascoside against *Staphylococcus aureus*. *J Ethnopharmacol* 1999;66:75–8.
- [73] Chiti F, Dobson CM. Protein misfolding, amyloid formation, and human disease: a summary of progress over the last decade. *Annu Rev Biochem* 2017;86:27–68.
- [74] Gioran A, Paikopoulos Y, Panagiotidou E, Rizou AEI, Nasi GI, Dimaki VD, et al. Beneficial effects of *Sideritis clandestina* extracts and sideridiol against amyloid β toxicity. *Antioxid Basel Switz* 2024;13:261.
- [75] Kurisu M, Miyamae Y, Murakami K, Han J, Isoda H, Irie K, et al. Inhibition of amyloid β aggregation by acteoside, a phenylethanoid glycoside. *Biosci Biotechnol Biochem* 2013;77:1329–32.
- [76] Shiao Y-J, Su M-H, Lin H-C, Wu C-R. Acteoside and isoacteoside protect amyloid β peptide induced cytotoxicity, cognitive deficit and neurochemical disturbances *in vitro* and *in vivo*. *Int J Mol Sci* 2017;18:895.
- [77] Andersen JK. Oxidative stress in neurodegeneration: cause or consequence? *Nat Med* 2004;10(suppl):S18–25.
- [78] Han Z, Wang B, Wen Y-Q, Li Y-N, Feng C-X, Ding X-S, et al. Acteoside alleviates lipid peroxidation by enhancing Nrf2-mediated mitophagy to inhibit ferroptosis for neuroprotection in Parkinson's disease. *Free Radic Biol Med* 2024;223:493–505.
- [79] Li M, Zhou F, Xu T, Song H, Lu B. Acteoside protects against 6-OHDA-induced dopaminergic neuron damage via Nrf2-ARE signaling pathway. *Food Chem Toxicol Int J Publ Br Ind Biol Res Assoc* 2018;119:6–13.
- [80] Guo D, Mao Q, Fang X, Huang L, Tian H, Yang W, et al. Synergistic modulation of microglial polarization by acteoside and ferulic acid via dual targeting of Nrf2 and ROR γ t to alleviate depression-associated neuroinflammation. *Adv Sci n.d.;n/a: e03889*.
- [81] Bardellini E, Amadori F, Schumacher RF, D'Ippolito C, Porta F, Majorana A. Efficacy of a solution composed by verbascoside, polyvinylpyrrolidone (PVP) and sodium hyaluronate in the treatment of chemotherapy-induced oral mucositis in children with acute lymphoblastic leukemia. *J Pediatr Hematol Oncol* 2016;38:559–62.
- [82] Campo G, Pvasini R, Biscaglia S, Ferri A, Andrenacci E, Tebaldi M, et al. Platelet aggregation values in patients with cardiovascular risk factors are reduced by verbascoside treatment. A randomized study. *Pharmacol Res* 2015;97:1–6.
- [83] Carmona F, Coneglian FS, Batista PA, Aragon DC, Angelucci MA, Martinez EZ, et al. *Aloysia polystachya* (Griseb.) *Moldenke* (Verbenaceae) powdered leaves are effective in treating anxiety symptoms: a phase-2, randomized, placebo-controlled clinical trial. *J Ethnopharmacol* 2019;242:112060.
- [84] Wu Y-T, Lin L-C, Sung J-S, Tsai T-H. Determination of acteoside in *Cistanche deserticola* and *Boschniakia rossica* and its pharmacokinetics in freely-moving rats using LC-MS/MS. *J Chromatogr B* 2006;844:89–95.
- [85] Wu L, Huang W, Peng K, Wang Y, Chen Q, Lu B. Enhancing the stability, BBB permeability and neuroprotective activity of verbascoside *in vitro* using lipid nanocapsules in combination with menthol. *Food Chem* 2023;414:135682.